Quantifying Changes in Glacier Thickness and Area Using Remote Sensing and GIS: Taku Glacier System, AK

by

Lara Hughes-Allen

A Thesis Presented to the
Faculty of the USC Graduate School
University of Southern California
In Partial Fulfillment of the
Requirements for the Degree
Master of Science
(Geographic Information Science and Technology)

May 2017

Table of Contents

List of Figures

List of Tables

Acknowledgments

I sincerely thank my thesis advisor, Steve Fleming, Ph.D., for his unwavering support, guidance, and understanding. Many thanks as well to Robert Vos, Ph.D., for helping build the foundation for this project and his participation on my thesis committee, as well as Su Jin Lee, Ph.D., for his participation on my thesis committee.

List of Abbreviations

AAR	Accumulation Area Ratio
ASTER	Advanced Spaceborne Thermal Emission and Reflection Radiometer
DN	Digital Number
ELA	Equilibrium Line Altitude
NIR	Near Infrared
SWE	Snow Water Equivalent
SWIR	Short-wave Infrared
TOA	Top of Atmosphere

Abstract

As anthropogenic climate change continues to accelerate, long-term and large scale monitoring of glaciers is crucial. The Taku Glacier offers a unique opportunity to apply remote sensing methods to a glacier with a long history of advance. The behavior of the Taku Glacier has been historically out of phase with regional climate and other proximate glaciers, which have undergone recent, and in some cases dramatic, retreat. Although remote sensing has been established as an effective tool for glacier monitoring, few studies have applied these methods to such a large glacier with so many diverse facies. This study establishes the effectiveness of using remote sensing to quantify long-term changes in glacier parameters including surface area, equilibrium line altitude (ELA), and accumulation area ratio (AAR) by combining a digitized historical topographic map, Landsat images, and a USGS DEM.

The results of the remote sensing analysis demonstrate significant downwasting and loss of mass at the margins of the glacier and areas of the glacier that are bounded by bedrock. In-situ monitoring has chronically underestimated this downwasting. This study quantified a substantial up glacier migration of the ELA and a corresponding reduction in AAR. Comparison of the AAR associated with each Landsat scene to the established equilibrium AAR for the Taku Glacier indicated that the Taku glacier has transitioned from a long period of positive mass balance to relative equilibrium. This transition likely presages a new period of retreat for the Taku glacier, which will have widespread consequences for downstream ecosystems and economies.

Chapter 1 Introduction

1.1 Research question and objectives

The goals of this research are: (1) quantify changes in the spatial extent, position of the equilibrium line, and corresponding accumulation area ratio (AAR) from 1973 to 2015 of the Taku Glacier in Southeast Alaska using Landsat remote sensing data; (2) evaluate changes from 1951 to 2015 in elevation of the glacier surface (as a proxy for thickness) using a historical topographic map and a 2014 USGS DEM; (3) compare the results of this remote sensing analysis with results from analysis of in situ data.

1.2 Motivation

Glaciers have been well established as valuable indicators of the severity of regional climate change and constitute an important part of the local and global hydrological cycle (Molina 2006). The health of glaciers and ice sheets has a significant influence on global sea level rise. A significant contribution to sea level rise comes from alpine glaciers, most of which have been identified to be declining in overall volume at an accelerating rate since 1990 (Larsen et al. 2006; Peduzzi et al. 2010). Although the total amount of ice stored in alpine glaciers is relatively small compared to the ice stored in Greenland and Antarctica, there is still significant potential to acutely affect sea level rise. The reduction of alpine glaciers, in Alaska and Canada specifically, is occurring so swiftly that glaciers in this region contributed more to sea level rise in the latter half of the 20th century than all the melting associated with the Greenland ice sheet (Larsen et al. 2006). Glaciers within Southeast Alaska and Canada are particularly susceptible to even minor changes in climate due to

their relatively low elevation and particular glacial geometry (Larsen et al. 2006). Consequently, robust monitoring of glaciers in Southeast Alaska is critical to understanding regional climate change as well as the effects of ice loss on global sea level rise and local hydrological systems.

Glaciers are a crucial part of the hydrological cycle in alpine regions and changes in their magnitude can have serious impacts on downstream systems (Figure 1). Glacier meltwater also sustains many alpine lakes and rivers, which support a diversity of flora and fauna. A decrease in the availability of this meltwater due to diminishing glacier volume will likely precede a marked reduction in the habitability of these alpine lakes and rivers. Additionally, numerous economies rely on these lakes and rivers for products like fish and fresh water, as well as hydropower. An estimated 75% of global freshwater is stored in glaciers, in combination with snow and ice surfaces. Approximately 16% of the world's population relies on glaciers for their fresh water supply (Peduzzi, Herold and Silverio 2009). Changes to these sensitive systems will, therefore, have far reaching impacts on the well-being of both nature and human livelihoods (Neal, Hood, and Smikrud 2010).

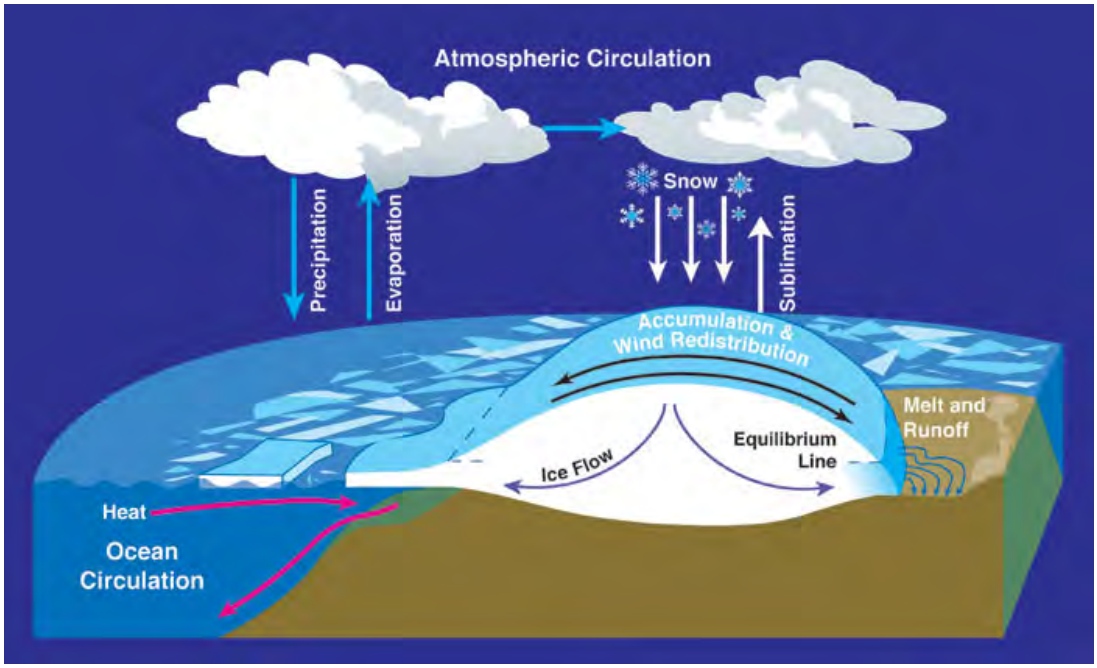

Figure 1 Schematic of glaciers and their effect on the hydrologic cycle.

Source: AntarcticGlaciers.org

Thinning and retreating of glaciers can also lead to significant changes in the hydrological cycle of the region. Initial increases in melting due to warmer temperatures are predicted to result in rapid increases in meltwater discharge that can result in flooding, changes in lake levels, and changes in the timing and intensity of meltwater availability to downstream ecosystems (Crossman, Futter, and Whitehead 2013). Once glacier thinning and retreat has progressed to the point where the regional glaciers are dramatically reduced in volume and extent, significant declines in the year-round amount of meltwater availability will likely occur. These changes might affect water quality in future years and the continual reduction in glacier volume will lead to an ultimate decrease or even elimination of meltwater availability (Crossman, Futter, and Whitehead 2013).

Furthermore, fresh water discharge from natural glacier melting during the summer is important to maintaining coastal circulation patterns as well as preserving biogeochemical fluxes to near-shore marine ecosystems (Crossman, Futter, and Whitehead 2013). Glaciers and icefields in Southeast Alaska contribute almost 50 percent of the available freshwater discharge into the Gulf of Alaska. Due to the complex interactions of glaciers with downstream hydrological systems, it is important to monitor changes in glacier parameters such as thickness and area extent of the glaciers to better predict how fresh water supply, flooding, and downstream ecosystems will be affected (Neal, Hood, and Smikrud 2010).

1.3 Study area: Taku glacier

Numerous studies use remote sensing to quantify changes in glacier parameters within the Alps and the Himalayan mountain systems, but there is a relative paucity of studies which use this methodology to study the glaciers of Alaska. As discussed in the previous section, glaciers that exist in Alaska and Canada are exceptionally sensitive to changes in temperature and precipitation.

The Taku glacier was chosen for study based on its location in southeast Alaska and its continued in situ monitoring since 1951. The Taku glacier has an area of roughly 700 km^2 and a length of approximately 60 km. The maximum estimated thickness of the Taku Glacier based on radio-echo sounding is 1,477 m with a minimum bed elevation at 600 m below sea level (Molina 2006). The radio-echo sounding was completed at five discrete points along the centerline of the main branch of the Taku glacier. The depth measurements at these points advance understanding of the bed topography only at these

specific points and extrapolation of these depths represents a gross generalization of the bed topography (Molina 2006). The mountains that lie buried beneath the ice of the Taku glacier system are relatively young and likely exhibit extreme variability in elevation and slope, among other characteristics. The bedrock topography of the Taku glacier is as irregular as any mountain range that is entirely visible. Therefore, it is extremely difficult to use point measurements to extrapolate to a comprehensive understanding of the bed topography that underlies any glacier. Additionally, radio-echo sounding measurements are generally limited to the centerlines of glaciers due to the heavy crevassing, prevalence of rockfalls, and other hazards that are characteristic the margins of glaciers. Extrapolation of these point measurements is especially unrealistic due to the large size of the Taku glacier system.

Besides its comparatively large size, the Taku glacier is also significant because its advance and retreat cycles have been out of phase with regional climate and the responses of other local glaciers. The Taku glacier advanced relatively consistently since 1850. The glacier experienced a period of stability between 1988 and 1999 and began advancing again during 2000 at a rate of about 30 cm per day (Figure 2). Between 2004-2006, the central part of the terminus continued its trend of advancement, but the lateral margins of the glacier experienced a small amount of retreat (Molina 2006). Preliminary data analysis shows that the terminus has been stable from 2012-2015 and has neither advanced nor retreated (McGee unpublished). It is important to note that terminus behavior is not necessarily coincident with overall accumulation or loss of mass and other indicators such as the position of the equilibrium line, changes in AAR and changes in elevation are more reliable indicators of general glacier condition (Dyurgerov et al. 2009).

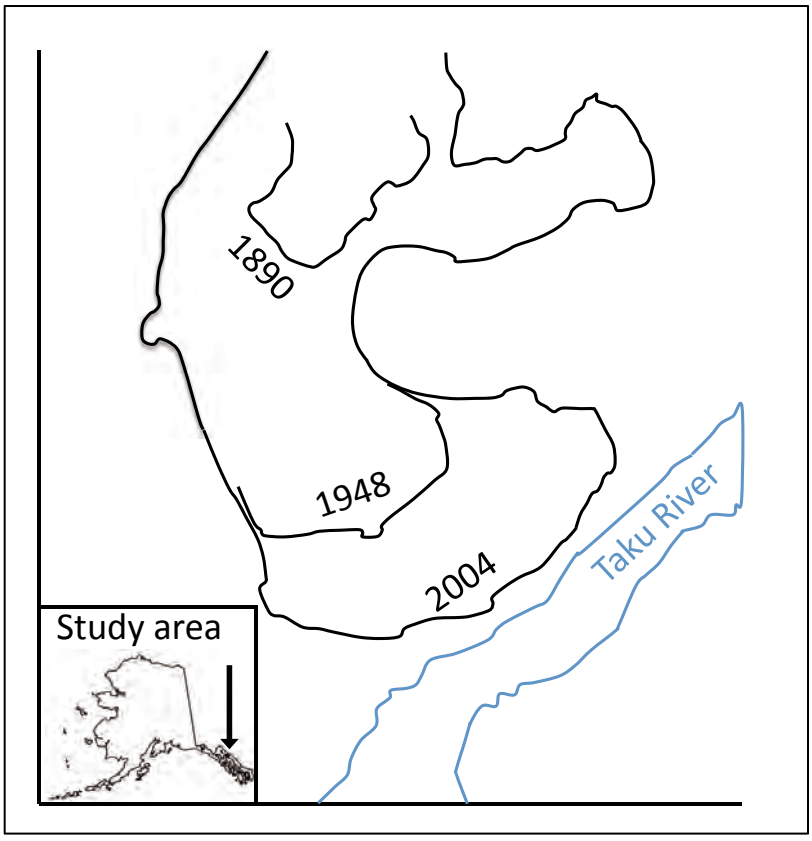

Figure 2 Image showing approximate locations of the Taku Terminus from 1890 to 2004. Adapted from Truffer et al. 2009

The Juneau Icefield Research Program (JIRP) has been collecting high-resolution digital GPS elevation data along 119 km of profiles across the entire Taku glacier system since 1999 (Figure 3). The availability of these in situ data offers an opportunity to validate by comparison the results of the remote sensing analysis. Few glaciers boast such a robust and long-term monitoring program and these data provide a unique opportunity for the comparison of the results of remote sensing analysis of elevation change with the results of in-situ analysis of elevation change (Figure 4). These methods facilitate a comprehensive study on the condition of the Taku glacier system in response to regional and global climate changes.

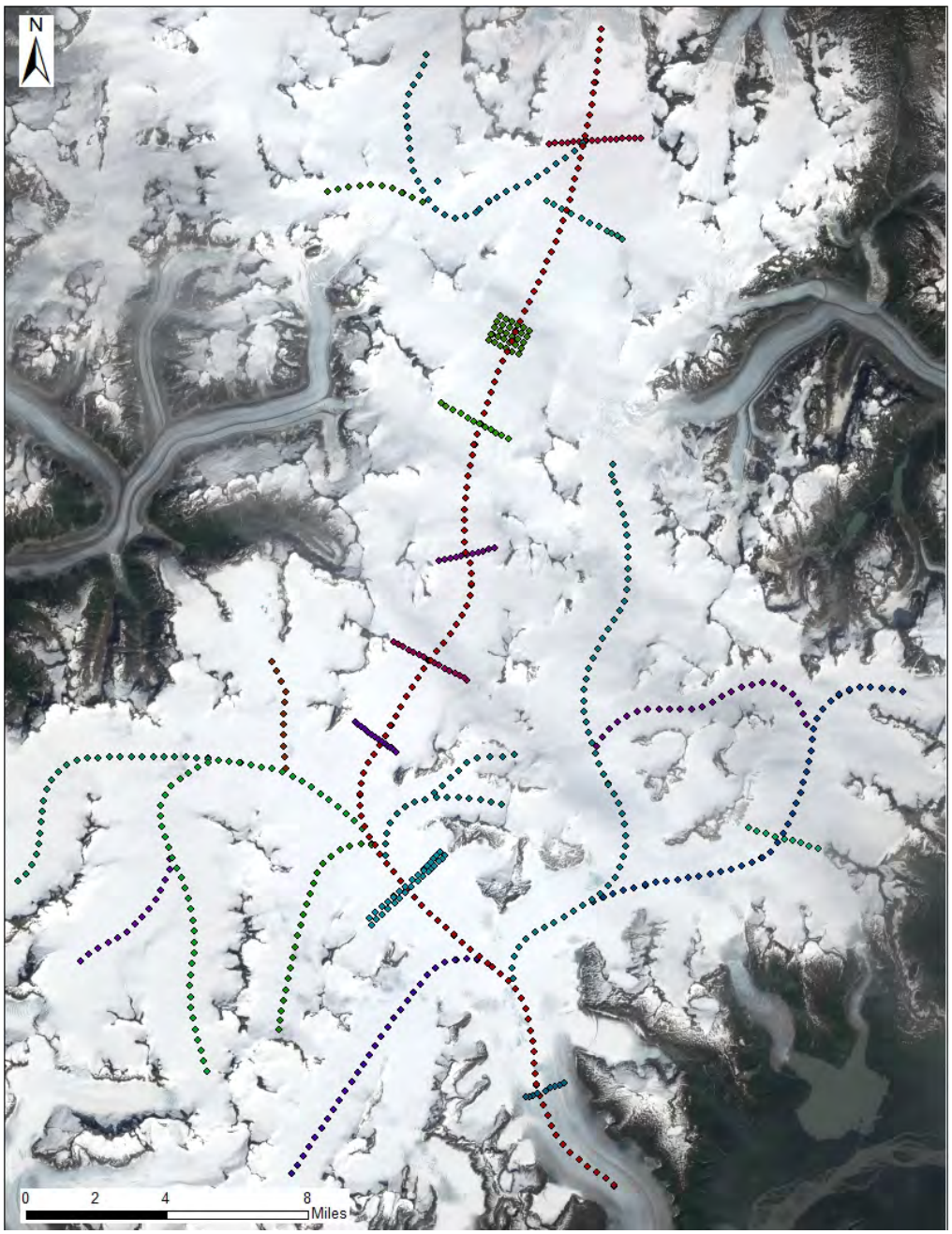

Figure 3 Map showing the distribution of survey profiles along the Taku Glacier system

Figure 4 Historical map of study area with 200 ft. contour intervals. General study area indicated by the blue square.

Chapter 2 Literature Review

Traditional glacier monitoring involves taking repeated, in situ measurements across the surface of a glacier. One of the most common metrics that is measured in situ is glacier surface balance and glacier mass balance. Surface mass balance is the net balance between the accumulation and ablation on a glacier's surface. Surface mass balance excludes any accumulation or loss of mass that might occur at the bed level. Mass balance is the total gain and loss of ice from a specific glacier system. Mass balance measured using the glaciological method is accurate at each site location, but spatially limited and extrapolation across the entire glacier introduces significant error that is especially acute on the Taku glacier given its large size (Pellikka and Rees 2010). Glaciers measured using this traditional glaciological method are often under sampled in many areas that are inaccessible to researchers (Zemp et al. 2013). Sources of error are systematically introduced based on the relative spatial representativeness of each point measurement and the method of interpolation between point measurements and extrapolation across the glacier surface.

The response time of a glacier's mass balance to changes in climate depends on the glacier's specific hypsometry, elevation, and location. Depending on these variables, there may be a significant lag time between changes in temperature and precipitation and perceptible changes in mass balance. Additional quantifiable parameters exist that offer a more immediate look at the response of a specific glacier to changes in climate, such as, equilibrium line altitude, and corresponding accumulation area ratio, as well as total glacier surface area. It has been well documented that remote sensing methods offer a

more effective and efficient technique to quantify changes in equilibrium line altitude, accumulation area ratio, and total glacier surface area (Haq, M Anul, and Menon 2012; Khalsa, Dyurgerov, Khromova, Raup, and Barry 2004; Peduzzi, Herold, and Silverio 2009; Pellikka, and Rees 2010; Rabatel et al. 2013). The ability to incorporate additional parameters beyond mass balance enables a more comprehensive understanding of a glacier's current and future response to changes in temperature and precipitation.

2.1 Glaciological Method of Glacier Monitoring

Historically, glaciers have been monitored using the glaciological method, which involves conducting in situ measurements and observations. However, the use of this glaciological method on most glaciers is extremely time consuming, expensive, and logistically impractical (Karimi et al. 2015; Peduzzi et al. 2009). Glaciers often exist in remote areas, experience unpredictable weather patterns and harbor numerous topographic hazards that make ground-based, in situ data collection difficult and costly. Ground-based data, while highly accurate, is also limited in spatial coverage (Bamber and Rivera 2007; Raup et al. 2007). For example, mass balance measurements conducted on the Taku Glacier represent approximately one survey site per 40 km^3 (Echelmeyer et al. 1996). The insufficiency of data collected in situ to successfully represent the diverse conditions across a glacier surface leads to excessive averaging and interpolation. The conditions across and between individual glacier surfaces are spatially heterogeneous, making it difficult to accurately interpolate from in situ point sampling (Bamber and Rivera 2007). Additionally, the repetition of ground-based measurements is often too infrequent to discern short-term patterns or distinguish between weather and climate effects (Bamber

and Rivera 2007; Kargel et al. 2005; Karpilo 2009). Based on the variability of response by glaciers to changing climate and weather patterns, it is important to establish spatially and temporally comprehensive monitoring on a significant percentage of glaciers globally.

Since 1960, in situ measurements have been conducted on approximately a dozen relatively small mountain and valley glaciers worldwide (Kargel et al. 2005; Zemp et al. 2013). It is estimated that over 100,000 glaciers exist globally (Molina 2006), making the continued monitoring of a few dozen glaciers unrepresentative of the state of glaciers overall (Kargel et al. 2005). A glacier's response to changes in climate and weather is greatly dependent on the glacier's specific physical characteristics such as hypsometry, accumulation area ratio, elevation, and location. The substantial variability in the physical characteristics of glaciers, even within close proximity to each other, results in inconsistent responses to similar changes in climate and weather. Glaciers within the same area can often exhibit markedly different stages of advance or retreat. For this reason, it is not possible to accurately extrapolate in situ measurements of a "benchmark" glacier to any other glaciers in the region or globally (Molina 2006).

2.2 Glacier Monitoring using Remote Sensing

Remote sensing data facilitates the monitoring of a greater number of glaciers in more variable regions that do not necessarily have to be accessible for field measurements (Bamber and Rivera 2007; Berthier et al. 2006; Dyurgerov et al. 2009; Kargel et al. 2005). The addition of more glaciers to long term monitoring programs will foster better understanding of glacier dynamics and enable more accurate predictions of glacier response to continued climate change (Karpilo 2009). Remotely sensed data offers a more

effective, cost efficient and time saving method to study glaciers. Satellite data also enables the analysis of several glacier parameters, including changes in glacier area extent, which are not possible with ground-based methods. Remote sensing offers an effective alternative to excessive interpolation and averaging of in situ data (Bamber and Rivera 2007; Berthier et al. 2006; Dyurgerov et al. 2009; Kargel et al. 2005).

It is crucial to understand changes in glacier extent because glaciers are typically bounded laterally by bedrock, which has a significantly lower albedo and thermal inertia compared to that of snow and ice. Rock gains heat more quickly relative to snow and has a high heat capacity, enabling the rock to continue to emit heat even at night. Eventually, melting of the glacier adjacent to the rock occurs, creating a gap between the rock and the ice. This gap is part of a positive feedback loop that generates more melting as more rock is exposed (Paul et al. 2007). Increasing the area of exposed rock adjacent to a glacier can also increase the amount of windblown dust that accumulates on the glacier, which lowers albedo and can cause accelerated melting of the glacier (Bøggild et al. 2010). A loss of surface area is not always accompanied by a similar loss in glacier surface elevation (thinning) or response at the terminus of the glacier. The margins of a glacier are characteristically hazardous and usually exhibit extensive crevassing and, in many cases, a significant bergschrund. The hazards associated with the margins of a glacier make in situ measurement collection unsafe and unlikely. Unlike remote sensing methods, traditional glaciological monitoring does not sufficiently account for this down wasting at the margins of the glacier. (Bamber and Rivera 2007; Paul et al. 2007).

2.3 Glacier Characteristics and Measuring

At the most fundamental level, glaciers are the result of snow accumulation during the winter season that survives melting (ablation) in the summer season. As snow accumulation continues, the weight of each subsequent winter snowpack forces the snow that exists beneath the surface to become denser and eventually turn to glacier ice. Snow that has survived for more than one winter season is called firn (also known as *névé*) and is considered to be a transitional stage between snow and glacial ice (Post and LaChapelle 2000). In order for a glacier to persist in a certain area, there must be sufficient snow accumulation during the winter to survive the summer melting season. Therefore, glaciers typically form in regions of characteristically wet and cold climates. Once sufficient snow has accumulated over the course of several seasons, the glacier begins to flow under its own weight (Karpilo 2009). Areas of persistent snow cover that do not flow are termed snowfields and are not considered to be part of the glacier system (Post and LaChapelle 2000) and are excluded from the calculated surface area.

2.3.1 Mass Balance of a Glacier

The thickness of a glacier is generally positively correlated with elevation. Areas of higher elevation receive more precipitation during winter accumulation and experience less melting during summer ablation due to characteristically lower temperatures. The accumulation area is the region of the glacier that experiences more snow accumulation than melting each year. The ablation zone is the lower elevation area of a glacier that sustains more summer ablation than winter snow accumulation. Although melting is the most common form of ablation, mass can also be lost through evaporation, sublimation and

in some cases calving. The boundary between the area of winter snow accumulation and the area of the glacier ice that is typically exposed during the ablation season is the transient snowline. Closely related to the snowline is the equilibrium line altitude (ELA), which is the elevation at which the accumulation area transitions to the ablation area (Figure 5) (Post and LaChapelle 2000). The total area of accumulation versus the total area of ablation is closely related to the mass balance of a glacier (Dyurgerov et al. 2009).

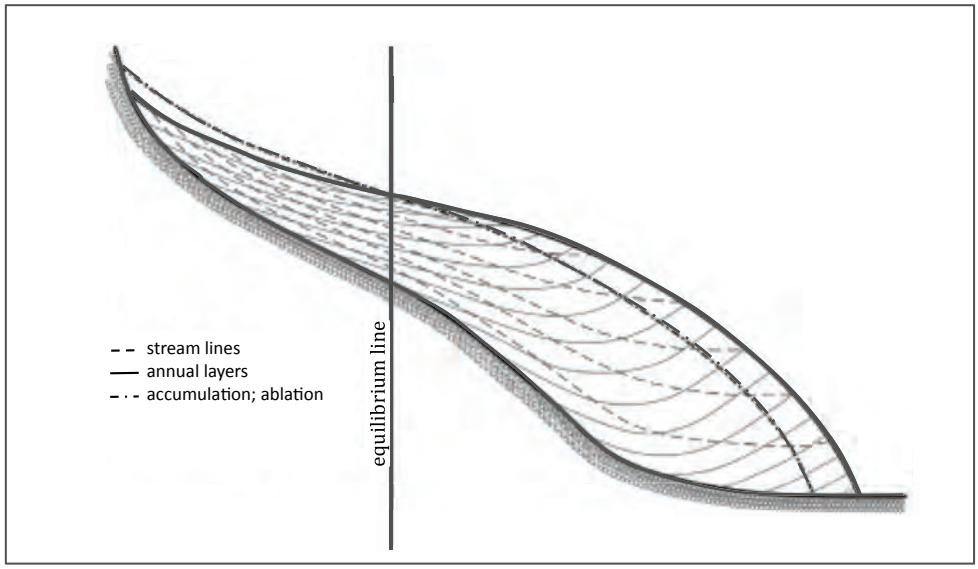

Figure 5 Finsterwalder's schematic of a glacier showing the accumulation of annual layers and the ELA

The difference between its yearly accumulation and yearly ablation is the mass balance of a glacier. Glaciers with a positive mass balance are growing, while glaciers with a negative mass balance are shrinking (Karpilo 2009; Paul et al. 2007). The mass balance of a glacier typically responds more immediately to changes in climate compared to other measureable metrics such as length and terminus position, which are characterized by a more delayed response (Raup et al. 2007).

Historically, the mass balance of a glacier has been determined by using numerous in-situ measurements of yearly accumulation and ablation. Yearly accumulation is measured at the end of the winter season, before summer melting occurs. At selected sites across the glacier, researchers dig down through the snow to last year's firn layer (Echelmeyer et al. 1995). The total depth of snow, as well as the density of the snow is recorded at each site. In order to normalize the different densities of snow, the snow depth is converted to the snow water equivalent. The snow water equivalent (SWE) winter precipitation is calculated using the specific snow density and the winter snow depth measured at each site (Larsen et al. 2006; Karpilo 2009; Meier et al. 2003; Molina 2006). Conceptually, if the entire snowpack were completely melted, SWE is equivalent to the depth of liquid water that would be produced (Criscitiello et al. 2010). This conversion allows for comparisons of snow depth between areas that experience significantly different types of snowfall (i.e. wet snow in a maritime climate versus dry snow in an inland climate).

The use of the glaciological method for determining mass balance invites sources of random and systematic error both during measurements in the field and during data analysis, specifically interpolation and extrapolation. Errors during field measurement can occur if an ablation stake has tilted or sunk, making accurate height measurements difficult. Similarly, tilt of the snow probe during seasonal snow depth determination can lead to inaccuracies in height determination. Difficulties and discrepancies in determining last years snow surface within the snow pack as well as density measurement errors can lead to inaccurate determination of seasonal accumulation. Additionally, the effectiveness of the point sampling network to capture the spatial variability of the surface balance can have significant implications for the accuracy of mass balance determination. Glacier facies with

unique surface balances, such as heavily crevasses areas, areas of debris cover, steep slopes, and avalanche zones, are typically under sampled due to inaccessibility and inherent danger (Larsen et al. 2006; Karpilo 2009; Meier et al. 2003; Molina 2006; Zemp et a. 2013). Given the relatively small sample size of sites across a glacier, the mass balance data collected at each site is interpolated between sample points and extrapolated across areas of the glacier that are not directly sampled (Pellikka and Rees 2010). Common interpolation methods include manually drawing contour lines between data points and the kriging interpolation (Hock and Jensen 1999).

Drawing contour lines between data points to extrapolate mass balance assumes a consistent mass balance gradient across the glacier and between mass balance points. If the mass balance points are irregularly spaced due to terrain and topographic considerations, the resulting extrapolated mass balance will be unrepresentative of the actual conditions on the glacier (Hock and Jensen 1999; Zemp et al. 2013).

The kriging method maintains the integrity of measured sample points and also takes into account distance between data points. This method dampens the effects of clustering by assigning less weight to points that are close together. Several different methods of kriging interpolation are available for glacier mass balance analysis including ordinary kriging with a nugget effect, ordinary kriging neglecting any nugget effect, and kriging with intrinsic function of first order (Hock and Jensen 1999). The nugget effect is generally appropriate for variables which experience rapid changes in value over a short distance. If no nugget effect is assigned, the values of the interpolated surface of the variable approach the actual values of the data points within a certain vicinity. The effect of a kriging

interpolation with no nugget effect assigned is a relatively smooth surface compared to a kriging interpolation with nugget effect. With respect to mean specific balance for a glacier, there is little variance between the results of the three different kriging methods (the results of these methods deviate from each other by approximately 0.1 m). In contrast, there can be significant variation between the results of the three types of kriging analysis with respect to the spatial distribution of the interpolated mass balance quantities (Hock and Jensen 1999). The differences in the spatial distribution of the mass balance quantities generated by these three methods have consequential implications when these values are used to determine the difference between a glacier's current state and its equilibrium state.

Mass balance measured using the glaciological method is accurate at each site location, but spatially limited and extrapolation across the entire glacier introduces significant error that is especially acute on the Taku glacier given its large size (Pellikka and Rees 2010). Glaciers measured using this traditional glaciological method are often under sampled in many areas that are inaccessible to researchers (Zemp et al. 2013). Sources of error are systematically introduced based on the relative spatial representativeness of each point measurement and the method of interpolation between point measurements and extrapolation across the glacier surface.

2.3.2 Remote Sensing and Mass Balance

As previously discussed, in situ monitoring of mass balance is, in most cases, costly, time consuming, dangerous and limited in spatial coverage (Bamber and Rivera 2007). However, several methods have been developed and implemented which bolster traditional glacier monitoring methods or offer an alternative to these methods (Karpilo

2009). Methods that do not utilize in situ measuring typically establish the mass balance of a glacier by determining the volumetric change of a glacier through time using airborne altimetry, topographic maps, and DEMs (from satellite or aerial imagery). These methods do not represent a direct observation of glacier mass balance because they rely on elevation as a proxy for thickness unless bedrock elevation has also been determined (Raup et al. 2007). A change in elevation is assumed to correlate directly with a change in mass given that there is insignificant change in bedrock elevation due to glacial rebound or tectonics and the density of ice has remained constant (Bamber and Rivera 2007). Tectonic uplift and glacial rebound are easily identifiable based on study site location. In areas where tectonic uplift or glacial rebound are likely to be occurring, the change in elevation directly related to these processes is probably less than a few centimeters per year, if not less. Changes in the densification of ice represent a similarly insignificant elevation loss of less than a few centimeters per year (Bamber and Rivera 2007).

Airborne altimetry involves the use of a nadir-point laser rangefinder mounted in an aircraft in conjunction with a gyro to monitor the orientation of the rangefinder and GPS for continuous tracking of the aircrafts position. Profiles are flown along the centerlines of the main trunk and significant tributaries of the glacier while elevation data is collected at designated intervals (Arendt 2006). However, as discussed in previous sections, analysis that is limited to centerline profiles is an insufficient method of glacier monitoring (Bamber and Rivera 2007). The benefit of airborne altimetry is the high accuracy of each elevation measurement, however several additional geodetic methods offer the ability to undertake a more comprehensive analysis of a glacier.

The improvement of the resolution and availability of satellite imagery has encouraged many researchers to utilize areal photogrammetry as a method for studying glacier change. ASTER has been collecting images over glaciated areas since December 1999. The visible and near infrared subsystem of the ASTER satellite is equipped with a nadir and backward looking telescope, which enables the creation of DEMs from ASTER imagery. Used in conjunction with several well-spaced ground control points (GCP), the accuracy of images produced using these methods is $\pm$15 m. These ground control points can be collected in situ using a high accuracy GPS (Berthier et al. 2007; Li et al. 2013) or, if in situ measurements are unavailable, GCP can be identified using a topographic map (Baolin et al. 2004; Khalsa et al. 2004). Static and easily identifiable features such as peak summits are a good choice for GCP derived from the topographic map (Khalsa et al. 2004; Paul et al. 2007). Once GCPs have been established and the image has been orthorectified, the ASTER derived DEM can be used for comparison with a digitized historical topographic map (Baolin et al. 2004; Barcaza and Aniya 2007; Peduzzi et al. 2009) or historical DEMs (Barcaza and Aniya 2007).

The use of historical topographic maps in the analysis of a glacier's changing mass balance significantly extends the timeline of the study, which is especially useful given the relatively slow response times of most glaciers to a changing climate. The historical topographic maps are prepared for analysis by georeferencing and resampling, to account for varying spatial resolutions of satellite derived DEMs. The contour lines of the topographic map are then manually digitized within the study area to derive a DEM (Peduzzi et al. 2009). The elevation of the surface of the glacier *(H)* is then compiled as an elevation time series, *H(t),* enabling the derivation of change in elevation through time

(dH/dt) by comparison of the digitized historical topographic maps with ASTER derived DEMs (Barcaza and Aniya 2007; Kargel et al. 2005; Khalsa et al. 2004; Peduzzi et al. 2009). The method of assessing elevation change as a proxy for changes in the mass balance of a glacier is fairly straightforward and useful. However, there are several additional glacial parameters that can be used in conjunction with mass balance, such as ELA and AAR, to yield a more comprehensive understanding of a glacier's reaction to a changing climate.

2.3.3 Equilibrium Line Altitude and Accumulation Area Ratio

Another common measurement used to assess the condition of a glacier is the accumulation area ratio (AAR), the total area of the accumulation zone divided by the total area of the glacier (Post and Lachapelle 2000). A glacier with an accumulation area that is between 50 and 60 percent of the entire glacier area exists in relative equilibrium and is neither growing nor shrinking (i.e., experiencing similar accumulation and ablation) (Dyurgerov et al. 2009; Karpilo 2009). When winter accumulation cannot persist through summer melting because of a reduction in precipitation, an increase in summer temperatures, or an increase in the length of the ablation season, the AAR is reduced and the glacier is no longer in equilibrium. If the AAR is reduced, there is typically a corresponding migration of the ELA to a higher elevation, often associated with glacier thinning and terminus retreat (Barcaza et al. 2009; Cheung-Wai et al. 2009; Dyurgerov et al. 2009).

The accumulation area ratio changes in conjunction with annual mass balance and tracking these changes over long-term time scales can yield information about glacier

condition and offer predictions about future glacier change. Dyurgerov et al. (2009) describe an effective method to quantify this index using Equation 1.

Equation 1

$$\alpha_d = (\langle AAR \rangle - AAR_0)/AAR_0 \quad (1)$$

In this case, $\langle AAR \rangle$ could be rewritten as AAR_i, where *i* is the year. If a glacier has a positive α_d, the accumulation area and likely the entire glacier area are becoming larger. The opposite is true of a negative α_d, in which case the glacier is likely retreating or will soon be in retreat (Dyurgerov et al. 2009). There is often a significant delay between temperature and precipitation changes and any observable changes in glacier area. These changes are often restricted to the ablation area and represent the glacier's adjustment to climate change (Leonard and Fountain 2003; Karpilo 2009). However, α_d represents a more immediate glacier response to shifts in temperature and precipitation (Dyurgerov et al. 2009).

Several methods of ELA monitoring exist and are employed respectively depending on study site characteristics. Repeat photography methodology has been utilized to study migrations of the ELA by establishing a photo location that affords a current and future view of the EL. The photo site is marked and imaging of the glacier coincides with the end of the ablation period is repeated periodically within the same time period (Karpilo 2009; Leonard and Fountain 2003). The photos are then used to visually estimate the location of the ELA or digitized to complete a more accurate estimation of the ELA (Karpilo 2009). If conditions on the glacier allow, the ELA may be also be established using in situ measurements (Echelmeyer et al. 1995). The ELA can also be determined by plotting mass

balance measurements on a map, then contouring the point measurements and estimating the ELA from these contours. The number and distribution of mass balance measurements limit the accuracy of this technique across the glacier. These techniques are employed on only a small number of glaciers and the use of remote sensing to establish ELA offers a more effective alternative to these traditional methods of glacier monitoring (Leonard and Fountain 2003).

As with monitoring changes in mass balance, the development and availability of high-resolution satellite images has greatly increased the accuracy of ELA and AAR analyses (Bamber et al. 2007). The satellite imagery is used to determine the location of the snowline at the end of the ablation season, but prior to any winter snow accumulation. A DEM is then utilized in conjunction with the established snowline to determine ELA (Barcaza and Aniya 2007). Based on the specific conditions of the study site, several different methods, including manual delineation and unsupervised classification, can be applied to identify the snowline.

Landsat and ASTER images are commonly used for this analysis because they are freely available and offer relatively high-resolution images (Barcaza and Aniya 2007). It is important that the images be relatively cloud free and be taken at a time when seasonal snow is absent and most or all of the summer melting has already occurred (Paul et al. 2007; Peduzzi et al. 2009; Pellikka and Rees 2010). Utilizing the Normalized Difference Snow Index (NDSI) and/or several additional band ratios can enhance the contrast between the accumulation and ablation zone and enable manual delimination of the snowline (Cheung-Wai et al. 2009). In some cases, such as when the study glacier is part of

a glacier system or icefield, manual delineation of the snowline is not a viable option (Barcaza et al 2009).

In a study on the Patagonian Icefield, Barcaza et al. (2009) use the NDSI with red (visible) and NIR bands to differentiate the accumulation and ablation zones. Using this technique, the accumulation area appears dark, while the ablation area appears bright. However, instead of manually digitizing the snowline, the authors also executed a K-means unsupervised classification on the NDSI images, which separated the pixels into one of five classes. The classes included: non-ice, shadow, bare ice, slush, and wet snow. The ablation area was defined as the aggregate of all pixels subsequently classified as bare ice. A DEM used to determine the altitude of the equilibrium line that was derived from the ASTER image. The vertical accuracy of the DEM was assessed by comparison of the off glacier areas, which shouldn't have experienced any significant elevation changes, with a historical topographic map. For this study, the same DEM derived from the 2003 ASTER image was used to determine the ELA for all five Landsat images. Rabatel et al. (2013) however, suggest using a DEM as close to the date of the satellite image as possible when determining ELA.

2.3.4 Satellite Considerations for Remote Sensing of Glaciers

Based on the shortcomings of traditional in-situ monitoring of glaciers discussed above, numerous researchers have employed remote sensing techniques in order to more effectively monitor long-term changes in the thickness, surface area and AAR of glaciers globally. The mapping of glaciers via remote sensing requires special consideration of satellite choice as multispectral sensors enable the mapping of small-scale glaciological

features as well as improved cloud cover discrimination (Pellikka and Rees 2010, 141). The available multispectral satellite sensors that are useful for glacier mapping are limited to Landsat TM/ETM+, SPOT HRV, and ASTER (Table 1).

Table 1 Specifications of the satellites commonly used in remote sensing of glaciers (V= visible, SWIR= short wave infrared, TIR= thermal infrared) (Adapted from Peduzzi and Rees 2010, 141)

Satellite	Landsat 5	Landsat 7	SPOT 4	Terra
Sensors	TM	ETM+	HRV	ASTER
Launch Date	1985	1999	1990	1999
Earth Distance (km)	705	705	830	705
Temporal resolution (days)	16	16	26	16
Image size (km x km)	185 x 180	185 x 180	60 x 60	60 x 60
Spatial resolution (m)	30, 120 (TIR)	30 (V, SWIR), 60 (TIR)	20 (V, SWIR)	15 (V), 30 (SWIR), 90 (TIR)

2.4 In-Situ Data Collection on the Taku Glacier

The use of the Taku glacier as a study site for utilization of satellite data to quantify changes in glacier thickness, ELA and AAR is unique because it is one of the few glaciers in the world with a long-standing in-situ monitoring program. This long-term data set enables a comparison between the result of the satellite data study and results from traditional in-

situ measurements. The comparison between traditional glaciological monitoring and remote sensing analysis will enable a better understanding of the errors and limitations of using remote sensing to monitor glaciers that would not otherwise be possible without long-term in situ data collection. This improved understanding of error and uncertainty in remote sensing analysis can then be extrapolated to other similar studies.

The Juneau Icefield Research Program (JIRP) has been completing field measurements of mass balance at approximately 17 sites across the Taku glacier since 1946. Summer ablation rates are determined at corresponding sites using ablation stakes. Measurement of summer ablation is less consistent and is only completed during about 20 percent of field seasons. Given the low number of mass balance sites and ablation stakes compared to the large size of the Taku Glacier, this method of mass balance determination is inadequate for the Taku glacier. The employment of 17 sites results in a paucity of data across the entire glacier. Additionally, winter mass balance measurements are taken after summer melting has already begun. Ablation rates are not monitored for the entire melt season and are interpolated based on regional temperature data (Criscitiello et al. 2010). These methods for monitoring the Taku glacier are not comprehensive and fail to sufficiently detect spatial variation across the glacier.

Chapter 3 Data and Data Corrections

The objective of this study is to evaluate the feasibility of using geodetic techniques to quantify changes in thickness and surface area of the Taku Glacier as well as migration of the ELA and change in the AAR. Remote sensing is superior to traditional in-situ monitoring methods and ArcGIS offers the ideal platform for analyzing and managing these images. Based on the shortcomings of traditional in-situ monitoring of glaciers, numerous researchers have employed remote sensing techniques in order to more effectively monitor glaciers long-term.

The mapping of glaciers via remote sensing requires special consideration of satellite choice as multispectral sensors enable the mapping of small-scale glaciological features as well as improved cloud cover discrimination (Pellikka and Rees 2010, 141). Relevant data with limited cloud cover were established, downloaded and imported into ArcGIS from USGS Global Visualization Viewer. To enable long term monitoring of changes in ELA, AAR, and surface area, scenes were chosen from approximately decadal intervals depending on the availability of low cloud cover images. Atmospheric corrections were completed prior to the execution of any analysis using the remotely sensed images. Additionally, the GLIMS outline for the Taku glacier did not accurately identify glacier areas that contribute mass to the main branch of the Taku glacier. The GLIMS outline for the Taku glacier system was modified for use in this study based on a posteriori knowledge as well as analysis of a USGS DEM to include all glacier areas that contribute mass to the main branch of the Taku glacier.

Several datasets are needed in order to quantitatively determine changes in glacier thickness and the location of the equilibrium line and determine the AAR (Table 2).

Table 2 Input datasets for satellite imagery

Satellite	Landsat 1	Landsat 4	Landsat 5	Landsat 7	Landsat 8
Sensors	RBV	MSS, TM	TM	ETM+	HRV
Launch Date	1972	1982	1985	1999	1990
Earth Distance (km)	917	705	705	705	830
Temporal resolution (days)	18	16	16	16	26
Image size (km x km)	170 x 185	170 x 185	170 x 185	170 x 185	170 x 185
Spatial resolution (m)	80	30 (V), 120 (TIR)	30, 120 (TIR)	30 (V, SWIR), 60 (TIR)	20 (V, SWIR)

All of the Landsat images were downloaded using the USGS Global Visualization Viewer (USGS Glovis). The study area corresponds to Landsat path 57 and row 19 (Figure 6) and is also contained within path 58 and row 19.

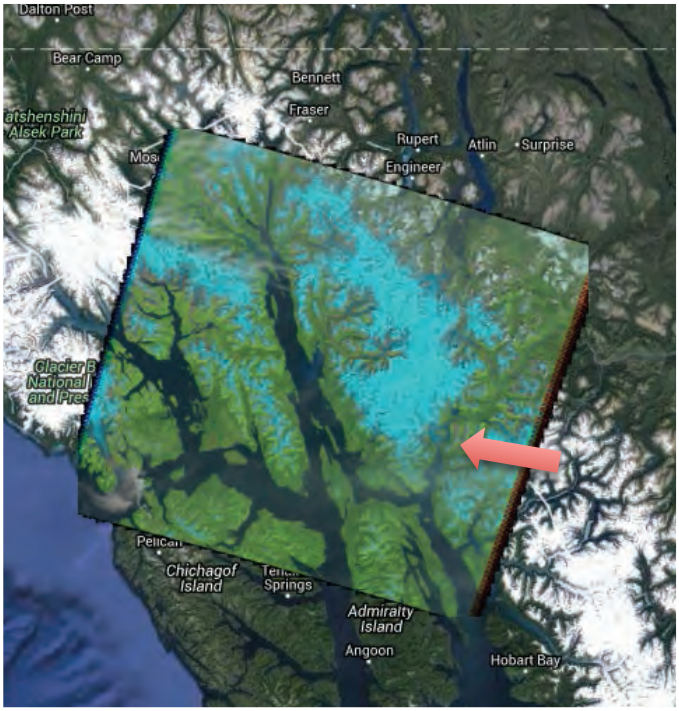

Figure 6 Image showing Landsat path 57 row 19 scene. Red arrow shows relative location of Taku Terminus.

Search specifications limited the scenes to include only images that have less than 20 percent of cloud cover and were taken at the end of the ablation period, but before the beginning of winter snowfall. This period consists of late-August through mid-October for southeast Alaska (Echelmeyer et al. 1996). Five Landsat images were chosen for analysis based on the need for low cloud cover images that were taken between late-August and mid-October, as well as the desire to have images that were relatively evenly spaced temporally (Table 3).

Table 3 Landsat images used for analysis.

Year	Month	Landsat Satellite	Percent Cloud Cover
1973	September	Landsat 1	10
1979	August	Landsat 2	13
1990	September	Landsat 5	12
2004	August	Landsat 5	0
2015	August	Landsat 8	15

The Landsat bands downloaded with each image correspond to specific types of reflected radiation (Table 4 and Table 5).

Table 4 Landsat 1-7 bands and their associated spectral characteristics

Band	Spectral Characteristics
Band 1	Blue
Band 2	Green
Band 3	Red
Band 4	Near Infrared (NIR)
Band 5	Shortwave Infrared (SWIR)
Band 6	Thermal Infrared
Band 7	Shortwave Infrared

Table 5 Landsat 8 bands and their associated spectral characteristics

Band	Spectral Characteristics
Band 1	Coastal aerosol
Band 2	Blue
Band 3	Green
Band 4	Red
Band 5	Near Infrared (NIR)
Band 6	Shortwave Infrared 1
Band 7	Shortwave Infrared 2
Band 8	Panchromatic
Band 9	Cirrus
Band 10	Thermal Infrared (TIRS) 1
Band 11	Thermal Infrared (TIRS) 2

A historical topographic map dated 1951 was also used to monitor changes in the elevation, and, by proxy, the thickness of the Taku glacier. The historical topographic map was freely available and downloaded from the USGS historical topographic map explorer (Figure 4).

Additional datasets are needed to compare the results of the remote sensing analysis with in situ elevation data. These in situ data are freely available from the Juneau Icefield Research Program and cover the entire Taku glacier system since 1993 (Figure 3).

3.2 Atmospheric corrections for remote sensing images

Despite careful screening of Landsat images for use in this study, there remains the need to complete several atmospheric corrections before the images can be used in the analysis. In addition to correction for clouds and cloud shadows, the digital numbers (DN) recorded by the sensor needs to be converted to surface reflectance (Liang et al. 2002). DN are not comparable between days because they represent the solar irradiance energy of a given pixel on the date of collection and are unitless. The value of the DN can be affected by the distance of the Earth from the Sun and well as the angle of incidence of the solar irradiance. Additionally, the scale of DN values is different for specific Landsat missions. Landsat 5 and Landsat 7 use scaled DN values of 0 to 255, while Landsat 8 uses scaled DN values of 0-4,095 (NASA 2011). These corrections follow the procedures described in Chander et al. 2009 and utilize the information provided in the metadata associated with each scene and can be completed within ArcMap using the *Raster Calculator* tool.

To transform the DN to top of atmosphere reflectance (TOA) values for Landsat 1-7, the DN first had to be converted to radiance, then subsequently to reflectance values.

DN to Radiance

$$= ((LMAX_{\lambda} - LMIN_{\lambda})/(QCALMAX - QCALMIN))*(QCAL-QCALMIN) + LMIN_{\lambda}$$

Where:

$LMAX_{\lambda}$ = spectral radiance scales to QCALMAX

$LMIN_{\lambda}$ = spectral radiance scales to QCALMIN

QCALMAX = the maximum quantized calibrated pixel value (typically 255)

QCALMIN = the minimum quantized calibrated pixel value (typically 1)

QCAL = digital number

Radiance to TOA Reflectance

$$= \pi * L_{\lambda} * d^2 / ESUN_{\lambda} * \cos \theta_s$$

Where:

L_{λ} = spectral radiance

d = Sun distance in astronomical units. Determined using Julian Day of the year on which the scene was acquired.

$ESUN_{\lambda}$ = mean solar exoatmospheric irradiances. Sensor specific based on high versus low gain.

θ_s = solar zenith angle

In order to convert the DN to TOA reflectance values for the Landsat 8 and Landsat 5 scene, the band specific reflectance for multi bands as well as the add band for each specific band (i.e. red, near infrared (NIR), or shortwave infrared (SWIR)) must be retrieved from the metadata.

DN Values to TOA Reflectance

= Band specific reflectance_Multi_Band x DN Values + Reflectance_Add_Band

The TOA reflectance is then used in combination with the sun elevation to correct for sun angle.

Correction for Sun Angle

= TOA Reflectance/ sin(Sun Elevation)

These calculations were completed for each band for every Landsat scene.

3.3 Glacier study area and Global Land Ice Measurements from Space

The Taku Glacier is part of the Juneau Icefield, which is comprised of numerous separate glaciers that at times converge or diverge. Unlike studies which examine a standalone glacier that does not receive mass input from other surrounding glaciers (Baolin et al. 2004; Berthier et al 2006; Haq et al. 2012; Khalsa, et al. 2004), care had to be taken to delineate a glacier study area that encompassed all areas that contribute mass to the Taku Glacier (Barcaza et al. 2009). A polygon shapefile of the Taku Glacier is available from the Global Land Ice Measurements from Space (GLIMS), however, it does not sufficiently account for all areas contributing mass to the Taku glacier and was subsequently modified.

Modifications to the outline of the Taku Glacier were made based on the historical topographic map, the USGS DEM and in situ knowledge of topography. The GLIMS Taku Glacier polygon includes an area in the northernmost part of the glacier that is known from

field observations and examination of the USGS DEM to flow away from the Taku terminus and toward Canada (Figure 13- see Appendix A; all figures from figure 13 onward are in appendices). The *Editor* function in ArcMap was used to manually redraw the northernmost boundary of the Taku glacier Additionally, the main branch of the Taku glacier is bifurcated above the terminus of the Hole-In-The-Wall Glacier (Figure 13).

The Taku glacier is more completely represented by adding the Hole-In-The-Wall glacier polygon, as well as the unnamed glacier to the east of the Hole-In-The-Wall glacier, to the Taku glacier polygon. The Echo glacier, which exists north of the Taku glacier, is also included in the Taku glacier polygon because examination of the historical topographic map and USGS DEM determined that it contributes mass to the main Taku glacier branch. Lastly, within the GLIMS glacier polygons, the rocky outcrops are excluded from the polygon area. However, these areas are important for analysis of down wasting of the glacier at the margins of these rocky outcrops (Paul et al. 2007). The polygons representing rocky outcrops were dissolved into the Taku glacier polygon using the Dissolve tool in ArcMap (Figure 14). The total area of the Taku glacier polygon is 689 km ^{2}. The approximate length of the main branch of the Taku glacier is 45 km.

Chapter 4 Methods

One benefit of using remote sensing in addition to, or in place of, traditional in situ monitoring is the ability to examine the long-term responses of glaciers to changes in climate through the lens of several distinct and complementary parameters that are not available using the glaciological monitoring method. Monitoring using the traditional glaciological method, is limited in its ability to consider multiple variables due to the time intensive, costly, and spatially limited nature of in situ fieldwork. Additionally, many remotely sensed imaging platforms have been collecting data since the 1970s. The availability of these long-term datasets enables researchers to effectively "look back in time" and consider past relationships between glacier activity and climate as well as establish persistent trends on glaciers that do not have established in situ monitoring programs.

This study utilizes remote sensing to consider the long-term trends of several different glacier parameters. After the completion of atmospheric corrections and post processing, the remotely sensed images were used to determine changes in ELA using band ratios and manual delineation. Surface area changes were determined using a modified GLIMS outline of the Taku glacier and unsupervised classification within ArcGIS to discriminate between bedrock surface and glacier surface. The determined surface area and ELA were then used to calculate AAR. The additional metric described by Dyurgerov et al. 2009, AAR_0, was determined using the calculated AAR for each scene and the value for the equilibrium state AAR as established by Pelto 2011. Several methods were used to convert the digitized contour lines from the historical topographic map to a digital

elevation model in order to identify the most effective interpolation method. These methods were adapted from several studies (Bamber et al. 2007; Baolin et al 2004; Cheung-Wai et al. 2009; Dyurgerov et al. 2009; Khalsa et al. 2004; Leonard and Fountain 2003; Pau et al. 2007; Raup et al. 2007), which utilize remote sensing to study specific glacier parameters. This study differs by combining several of these metrics as well as quantifying snow surface loss within the accumulation zone (Figure 7).

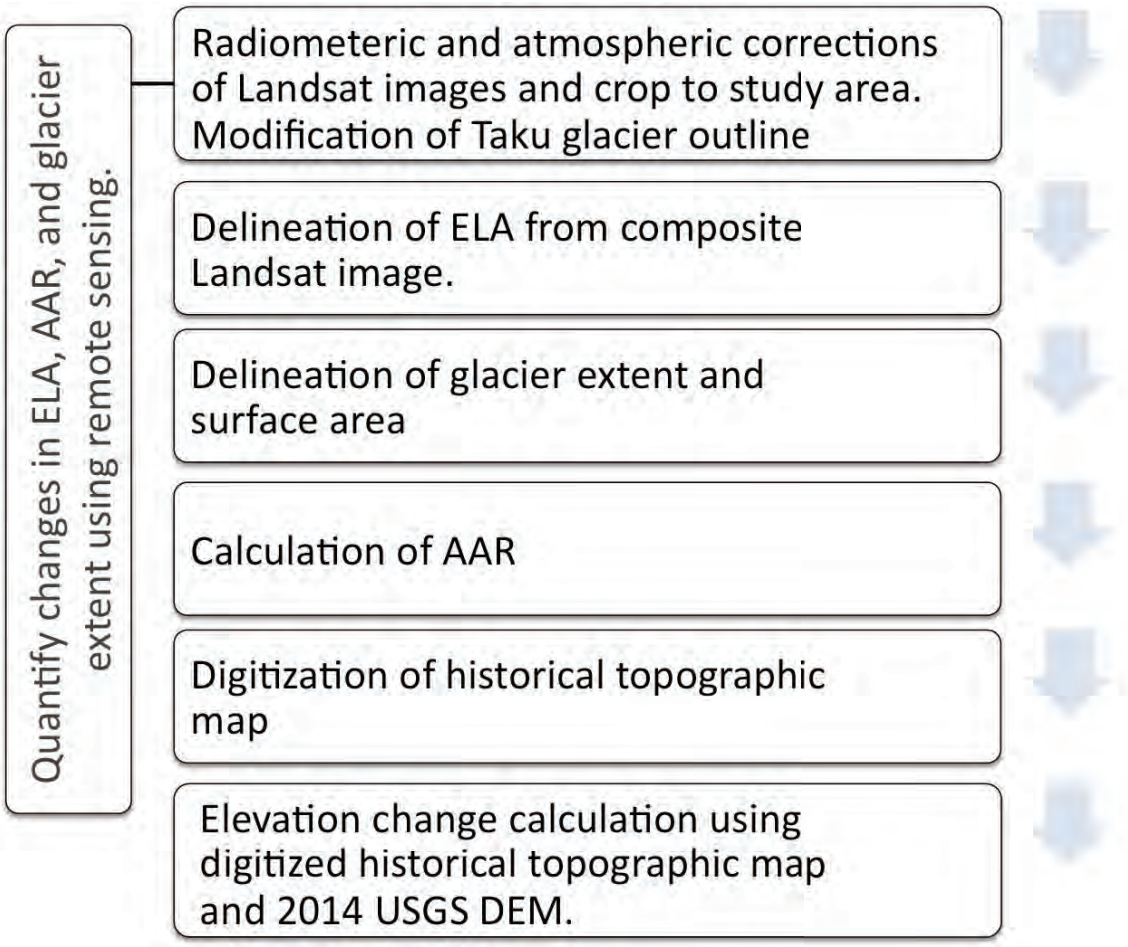

Figure 7 Methodological workflow: Using remote sensing to quantify changes in ELA, AAR, and glacier extent.

4.1 Delineation of ELA

The delineation of the ELA utilizes the lower albedo (50% or less) of ice and firn, which are characteristic of the ablation zone, compared to the higher albedo (60% to 90%) of seasonal snow in the accumulation area. Based on these differences, the SLA can easily be determined remotely, and because the remote images are taken from the end of the melt season, the SLA is consistent with the ELA (Barcaza et al. 2009; Leonard and Fountain 2003; Rabatel et al. 2013).

A composite image was created using green, near infrared, and short wave infrared bands, which was then used to manually delineate the equilibrium line (Figure 15) (Rabatel et al. 2013). Once the relative location of the equilibrium line was determined for each scene, the USGS DEM was used in conjunction with the *Add Surface Information (3D Analyst) tool* to determine information about the elevation of the equilibrium line. A bilinear interpolation method was used, as the input surface was a raster dataset. The data generated using this tool included: mean elevation, maximum elevation, minimum elevation, length, minimum slope, maximum slope, and average slope. The identification of the mean equilibrium line elevation facilitates easy comparison of the position of the ELA between scenes and offers a comprehensive look at the migration of the ELA through time (Rabatel et al. 2013).

4.2 Delineation of glacier extent and surface area

The glacier extent associated with each Landsat scene was calculated from the corrected images. A composite image was created for each scene using band 4, band 5, and band 6 for the 1973 Landsat scene (Paul et al. 2009). A false color composite (band 5, band 4, and band 3) was used for all subsequent Landsat scenes (Paul et al. 2009).

Experimentation with both supervised and unsupervised classification revealed that areas of the ablation zone with low reflectance could not be successfully distinguished from areas of rocky outcrops within the accumulation zone. To remedy this, the composite image for each scene was divided into two sections representing the accumulation zone and ablation zone. The ELA associated with each scene was used as an input for the equation DEM$\geq x$, which was completed using the *Raster Calculator (Spatial Analyst)* tool. In this case, DEM represents the 2014 USGS DEM and *x* is the ELA associated with each Landsat scene. This equation produced a binary raster where 1 represented the accumulation zone and 0 represented the ablation zone (Figure 16).

The accumulation and ablation zone raster was converted to a polygon using the *Raster to Polygon (Conversion) tool.* A separate layer was generated for the accumulation zone and ablation zone respectively using the *Select by Attributes function* and then the *Create Layer from Selected Feature function.* The composite image was then divided into separate accumulation zone and ablation zone facies using the polygon representing each facies and the *Extract by Mask (Spatial Analyst) tool*.

An unsupervised classification scheme was utilized for the accumulation section and the ablation section, respectively, to facilitate the delineation of the glacier area from surrounding bedrock. There are many different facies that fall under the umbrella of the accumulation and ablation zone, respectively. Within the ablation zone, for example, there may be areas that consist mostly of clear blue ice. Nearby, there may be areas that are more characterized by ice covered by a layer of dust or debris. Closer to the transition zone between the ablation area and accumulation area, but still within the ablation zone, there may an area of mixed firn and ice. All of these facies have specific albedos that vary slightly from each other. Due to the natural variation in albedo of the different facies that are present across the glacier, several separate classes were used to capture the heterogeneity present within the ablation zone, accumulation zone, and bedrock. For the 1973, 1979, 1990 and 2015 ablation zone and accumulation zone scenes, eight separate classes were needed to accurately differentiate the glacier surface from surrounding bedrock (Figure 17). The August 15, 2004 scene required 12 separate classes to accurately determine glacier surface versus surrounding rock in both the ablation zone and accumulation zone.

The raster generated by the unsupervised classification was then visually compared to the composite image to determine which classes generated by the unsupervised classification are associate with the glacier surface category or the bedrock category, respectively. The *Reclassify (Spatial Analyst) tool* was used to convert the multiple class raster to a raster containing only one class representing the glacier surface and the second class represented the surrounding bedrock (Figure 17). These methods were completed separately for the accumulation zone and ablation zone.

Similar steps were followed to classify the accumulation zone. The composite image was used as an input for the unsupervised classification, which utilized eight separate classes (excluding the 2004 Landsat scene which utilized 12 classes) (Figure 19).

The raster created by the unsupervised classification was then reclassified to represent rocky outcrops and glacier surface only (Figure 20).

In the 2004 and 2015 Landsat scenes, areas snow free ice (bare ice) became more prevalent in the accumulation area and was included in the bedrock facies category because it is abnormal for there to be bare ice within the accumulation zone (Dyurgerov et al. 2009; Leonard and Fountain 2003; Paul et al. 2009). Bare ice is typically characteristic of the ablation zone and its presence in the accumulation zone indicates that certain areas of the accumulation zone are experiencing more melt than accumulation. This additional melt is not represented by the migration of the equilibrium line, but remains an important trend that should be quantified (Leonard and Fountain 2003). The increasing prevalence of bare ice is apparent in Figure 21, which shows a composite image of the 2004 Landsat scene.

To determine the complete glacier surface area, the number of pixels of glacier surface associated with the accumulation zone and ablation zone were combined for each scene. This number was then multiplied by the pixel size specific to each Landsat scene to generate the total glacier surface area (Rabatel et al. 2013).

4.3 AAR Calculation

Once the position of the ELA was determined and the total glacier surface was calculated for each scene, it was possible to determine the accumulation area ratio. In order to complete analysis of the entire glacier surface, as opposed to the accumulation zone and ablation zone separately, a new raster dataset was created to represent the complete glacier surface. The raster datasets representing the glacier surface and bedrock areas of the accumulation zone and ablation zone respectively were mosaicked together into the new raster dataset using the *Mosaic (Data Management) tool.* This new complete raster dataset was then converted to a polygon using the *Raster to Polygon (Conversion) tool*. In order to maintain the integrity of the glacier and bedrock surfaces, the polygons were not simplified.

A new layer representing the glacier surface only was created using the *Select by Attribute function* and then the *Create layer from selected features function.* This new polygon layer representing the entire glacier surface of the Taku glacier was used to create a new modified USGS DEM layer of the same extent using the *Extract by Mask (Spatial Analyst) tool*. In order to determine the area above the mean equilibrium line altitude, the new DEM layer was used as the input surface for the *Surface Volume (3D Analyst) tool*. The average equilibrium line altitude was used as the input for plane height and the reference plane was set to ABOVE. The AAR was then calculated using the total glacier surface area and the total glacier surface area above the mean equilibrium line altitude (Dyurgerov et al. 2009).

The glacier index described by Dyurgerov et al. 2009 was also calculated for each Landsat scene. The approximate equilibrium AAR for a non-calving glacier such as the Taku glacier is established to be 0.67 (Pelto 2011). α_d was calculated using Equation 1, with the equilibrium AAR value of 0.67 and the AAR determined above. α_d facilitates easy comparison of the glacier state at the time of each Landsat scene and the equilibrium glacier state.

4.4 Digitization of Historical Topographic Map

The historical topographic map was manually digitized in ArcMap to enable comparison between the elevation of the glacier in 1951 and the elevation of the glacier in 2014 from the USGS DEM. The first step in digitizing and georeferencing the historical topographic map was to convert it from its PDF form to a TIFF file so that it could be imported into ArcMap. This conversion was done using pdf-online.com, a freely available online service. Once the TIFF of the historical topographic map was imported into ArcMap, it was assigned a spatial coordinate system (WGS_1984_UTM_Zone_8N) using the *Project (Data Management) tool.* The latitude and longitude grid ticks were then used to georeference the map. Twenty ground control points were utilized. All of the contour lines were manually digitized (Peduzzi et al. 2009) at the 200 ft. contour interval within the area that corresponded to the glacier study area (Figure 22).

Several different methods were initially used to convert the digitized contour lines to a raster format for comparison to the USGS DEM in order to determine which method produced the most accurate raster. The first method involved the standard *topo to Raster* tool within ArcMap. The digitized contour lines were used as an input for the *Topo to Raster*

tool within the spatial analyst toolset to create a DEM of the 1951 elevation of the Taku glacier (Figure 23). Due to the differences between glaciers and traditional watersheds, drainage was not enforced (Peduzzi et al. 2009). Lastly, the *Times (Spatial Analyst) tool* was used to convert the DEM from feet to meters. The USGS DEM was used to create the hillshade because the digitized contours were limited to glacier area only and did not include the rocky outcrops.

The second method to create a DEM of the 1951 topographic map utilized a triangulated irregular network that was created from the digitized contour lines using the *Create TIN* tool (Figure 24). This tool was run twice to assess the affect of using constrained or no constrained Delany triangulation.

There was no perceivable difference between the two iterations of this tool. The output TIN of this tool was then used as an input for the *TIN to Raster* tool. Two iterations of this tool were completed using natural neighbors and linear interpolations respectively. The terminus position of the Taku glacier has advanced significantly since 1951, which likely accounts for the DEM generated using IDW interpolation not extending into the full terminus area as depicted by the glacier outline (Figure 25).

Lastly, the contour lines were converted to points and interpolated using IDW and Kriging interpolation methods. The contour lines were converted to points using the *Generate points along a line* tool. The point placement was determined by percentage at 10 percent. For the IDW interpolation, the exponent of power was left as the default value of two and the number of points within the search radius was changed to six points. This IDW interpolation generated small areas of inconsistently low elevation within the

accumulation area that is not consistent with the historical topographic map or glacier dynamics in general (Figure 26).

The Kriging interpolation was run as a universal kriging and an ordinary kriging. The semivariogram model used for the universal kriging was linear with linear drift. The number of points within the search radius was similarly reduced to six points. The universal kriging interpolation method created areas of incongruously low elevation within the glacier areas, especially the accumulation zone (Figure 27). This interpolation also produced a DEM raster that was significantly more variable in elevation when compared to the relatively linear increase in elevation up glacier as described by the historical topographic map.

Lastly, the points were interpolated using an ordinary kriging interpolation. The semivariogram model used for the ordinary kriging was spherical. The number of points within the search radius was similarly reduced to six points. This interpolation method produced a DEM raster that showed a more regular increase in elevation up glacier compared to the universal kriging interpolation method (Figure 28). However, there are still some areas of low elevation adjacent to areas of higher elevation within the accumulation zone, which is not consistent with the historical DEM of glacier dynamics in general.

4.5 Elevation change on the Taku Glacier

The most recently available DEM for the Taku glacier area during the summer months is a USGS DEM from 2014. The USGS DEM was published on July 15, 2014, which is

before the completion of the melting period, and it is possible that some seasonal snow existed (Bamber and Rivera 2007). The difference in elevation of the Taku glacier from 1951 to 2014 was determined using the digitized historical topographic map and the USGS DEM. No resampling of either DEM was necessary as the pixel size for both DEMs was the same. The USGS DEM was limited to the Taku glacier study area using the *Extract by Mask (Spatial Analyst) tool.* The *Minus (3D Analyst) tool* was used to subtract the elevation of the 1951 DEM from the 2014 USGS DEM (Figure 8).

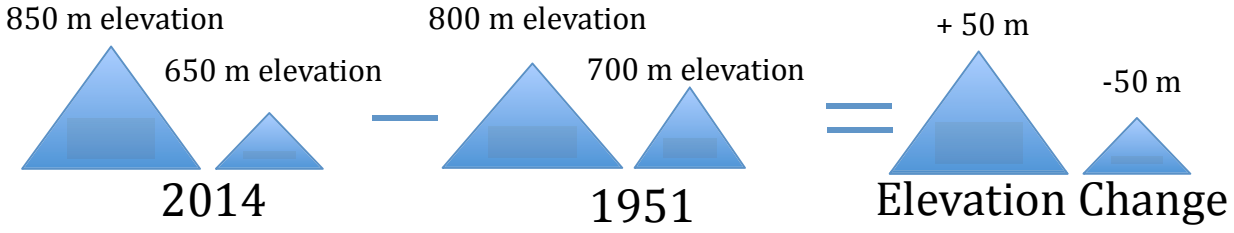

Figure 8 Schematic describing elevation change calculation.

In addition to the above methods, a second analysis was carried out which attempted to exclude the bedrock surfaces from analysis. Polygons were drawn around the bedrock areas using the historical topographic map and the *Drawing toolbar*. A second polygon was drawn to encompass the entire Taku glacier outline. The bedrock polygons were then removed from the study area polygon using the *Remove overlap function* on the *Drawing toolbar* (Figure 29).

The general study area polygon excluding bedrock surfaces and the *Clip (Analysis) tool* were then used to modify the Taku glacier outline shapefile so that it also excluded bedrock surfaces. The Taku glacier outline excluding bedrock surfaces was then used as an input for the *Extract by Mask (Spatial Analyst) tool* so that the USGS DEM. The digitized

contours lines of the historical topographic map were interpolated a second time using the outline of the Taku glacier excluding bedrock to limit the processing extent. The *Minus (3D Analyst) tool* was used to subtract the new USGS DEM from the new historical DEM.

4.6 In situ elevation analysis

In situ elevation data is only available from 1999 to 2015. Based on this data limitation, it is not possible to compare the 1951 topographic map to USGS DEM analysis to the same analysis generated using in situ data. Instead, the 1951 DEM was compared to a DEM created from the in situ elevation profiles from 2014. The results of this analysis were then compared to the elevation change determined using the 1951 DEM and the 2014 USGS DEM. Eleven individual GPS survey profiles that corresponded to the Taku glacier study area were merged into a single dataset using the *Merge (Data Management) tool* (Figure 30). These profiles included eight longitudinal profiles and three transverse profiles. No GPS survey profile is available for the lower ablation zone (Figure 30).

These GPS points were interpolated using the *Spline (Spatial Analyst) tool* to create a DEM (Figure 31). The processing extent was limited to the glacier surface only (Figure 29) in an effort to minimize the effects of the un-digitized rocky outcrop areas of the historical DEM. The 1951 DEM was then subtracted from the DEM created from in situ GPS data to determine overall change in elevation from 1951 to 2014.

Chapter 5 Results

This chapter presents the key findings of the comprehensive remote sensing analysis of the Taku glacier. The analysis of the glacier parameters considered in this study showed a transition from a state of positive mass accumulation to an equilibrium state. Total glacier surface area declined from 1973 to 2015 accompanied by an increase in bedrock area and bare ice in the accumulation zone. The equilibrium line migrated consistently up glacier during this same time period, which resulted in a reduction of the accumulation area ratio. Comparison of the accumulation area ratio for each scene to the equilibrium accumulation area ratio specific to the Taku glacier showed a shift from positive mass balance between 1973-2004 to an equilibrium state in 2015. No observable trends resulted from the elevation change analysis.

5.1 Glacier extent

The Taku Glacier experienced an overall decline in total glacier surface area from 1973 to 2015 and an increase in total bedrock (Table 6). There was, however, a period of increase in total glacier surface from 1973 to 1979 (Table 6).

Table 6 Total glacier surface, bedrock, and percent glacier surface for each Landsat scene.

Landsat Scene	Total Glacier surface (km^2)	Total Bedrock (km^2)	Percent glacier surface
1973	593.2	96.2	86%
1979	631.5	57.8	92%
1990	581.1	108.2	84%
2004	566.0	123.4	82%
2015	524.7	164.8	76%

Following an increase in total glacier surface from 1973 to 1979, the most significant decline in total glacier surface area occurred between 1979 and 1990 (Figure 9). Some of the area designated as bedrock in the 1990 Landsat scene represents bare ice in the accumulation area. A complete loss of snow surface in the accumulation area represents a loss of glacier surface that is equivalent to the exposure of bedrock in the accumulation area (Dyurgerov et al. 2009; Leonard and Fountain 2003; Paul et al. 2009). Bare ice is expected in the ablation area at the end of the melt season and is represented as glacier surface.

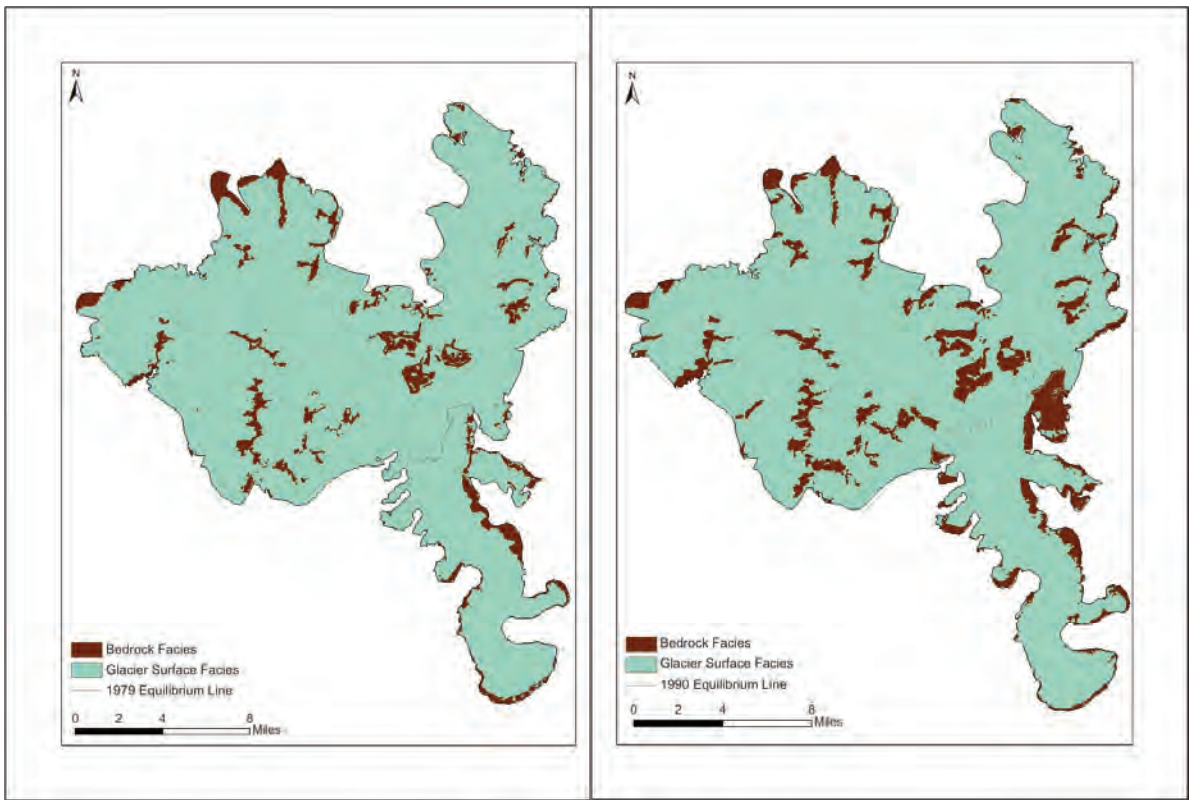

Figure 9 Glacier surface and bedrock designation for 1979 (left) and 1990 (right) Landsat scenes.

The relationship between glacier surface and total bedrock and bare ice was also analyzed for the accumulation area specifically. The overall decreasing trend from 1973 to 2015 is very similar to the trend shown by the entire glacier (Table 7). The gross decline is more significant compared to the total glacier with the percent snow cover for 2015 at 70%.

Table 7 Total snow surface, bedrock and percent snow cover for the accumulation area for each Landsat scene.

Landsat Scene	Glacier Surface (km^2)	Total Bedrock and bare ice (km^2)	Percent snow
1973	504.8	85.5	86%
1979	464.1	43.8	91%
1990	426.5	79.5	84%
2004	396.7	109.4	78%
2015	356.7	149.4	70%

5.2 ELA and AAR

The equilibrium line altitude for the Taku glacier experienced migration up glacier from 1973 to 2015 (Table 8; Figure 10). The most significant movement of the equilibrium line occurred between 1973 and 1979 with the equilibrium line moving 111 meters up glacier. Movement of the equilibrium line remained relatively constant from 1979 to 2015 with an average movement up glacier of 69 m $\pm$ 4 between Landsat scenes (Table 8; Figure 10).

Table 8 Mean equilibrium line altitude and difference from 1973 equilibrium line altitude associated with each Landsat scene.

Landsat Scene	Mean EL Altitude (m)	Elevation difference from previous scene (m)	Difference from 1973 ELA (m)
1973	801	-	-
1979	912	111	111
1990	977	65	176
2004	1,045	68	244
2015	1,120	75	319

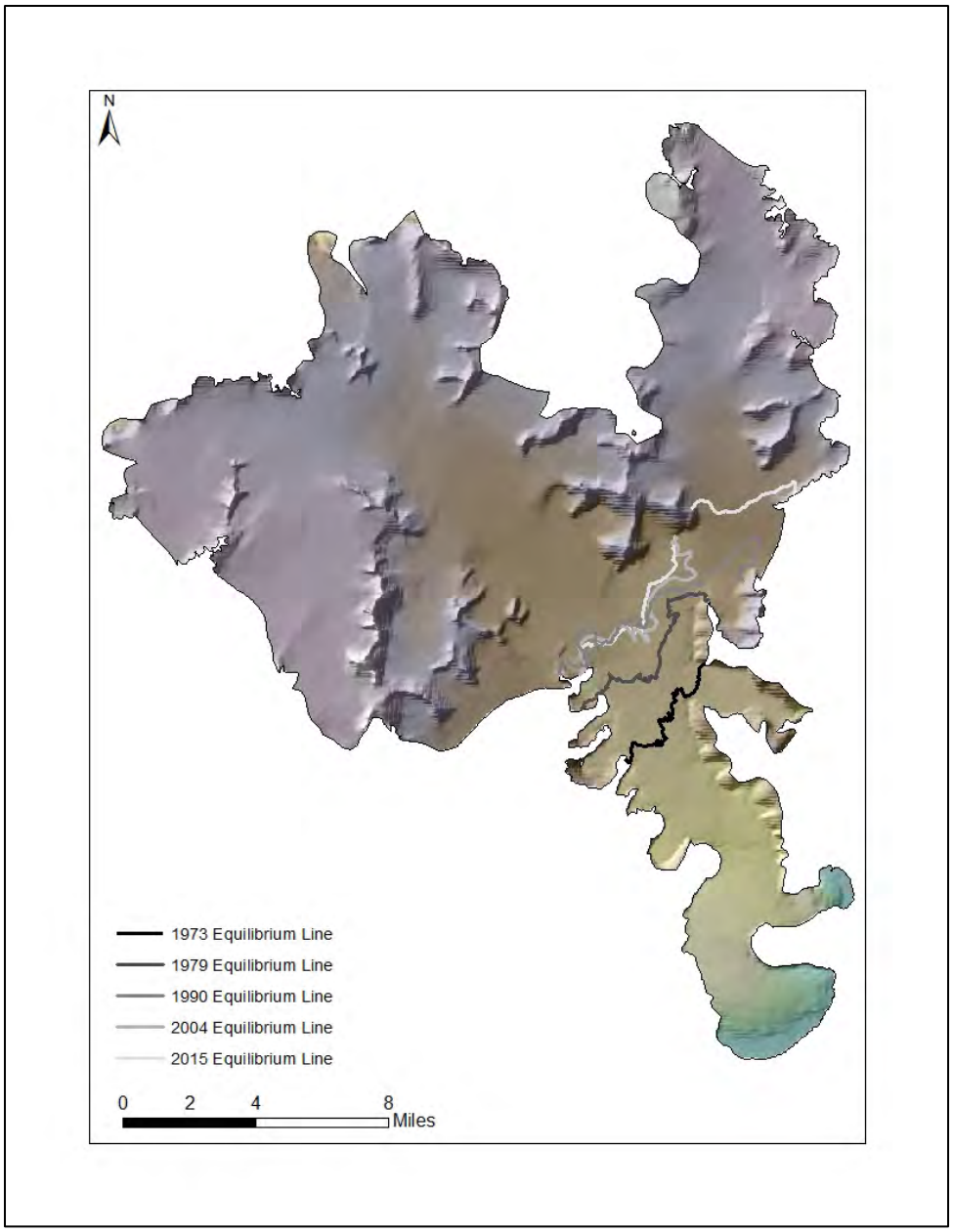

Figure 10 Map showing position of equilibrium lines for each respective Landsat scene.

The accumulation area ratio also experienced consistent decline from 1973 to 2015 (Table 9). The greatest reduction in AAR occurred between Landsat scenes 2004 and 2015 with a 0.7 reduction in AAR. The difference in AAR between all other scenes was 0.4.

Table 9 Total area above equilibrium line and corresponding AAR for each Landsat scene.

Landsat Scene	Total Area Above ELA (km^2)	AAR
1973	594.9	0.86
1979	561.9	0.82
1990	539.9	0.78
2004	510.7	0.74
2015	516.2	0.67

Analysis of α_d showed that the Taku glacier remained in a state of positive mass balance during the time period of this study based on the positive α_d values calculated for each Landsat scene (Table 10) (Dyurgerov et al. 2009). However, each successive Landsat scene is associated with a smaller α_d and the α_d value for 2015 reached 0.0.

Table 10 AAR_i and α_d for each Landsat scene.

Landsat Scene	AAR_i	α_d
1973	0.86	0.28
1979	0.82	0.16
1990	0.78	0.13
2004	0.74	0.10
2015	0.67	0.0

5.3 Elevation Change on the Taku glacier from 1951-2014

In order to better understand the results of the elevation change analysis, statistics for the DEMs created for each of the elevation change analyses are given in Table 11.

Table 11 Statistics for each of the DEMs created for the elevation change analysis.

DEM	Mean Elevation (m)	Minimum Elevation (m)	Maximum Elevation (m)	Standard Deviation (m)
1951 Historical DEM (including rocky outcrops)	1149	0	1782	350
1951 Historical DEM (glacier surface only)	1119	0	1782	352
2014 USGS DEM (including rocky outcrops)	1199	-0.3	2072	365
2014 USGS DEM (glacier surface only)	1183	-0.3	2073	372
2014 GPS Interpolated DEM	1205	342	1714	286

It is difficult to determine from the DEM comparison whether the Taku glacier experienced elevation gain or loss during the period between 1951 and 2015. The problem of the non-digitized rocky outcrops is especially significant for the analysis using the complete DEMs. Substantial elevation gain is shown where the bedrock protrudes out of

the glacier because the rocky areas were not digitized on the historical topographic map, but are included in the 2014 USGS DEM (Figure 32). The mean elevation change across the glacier from this analysis is an increase of 50 m $\pm$ 152.

The analysis of elevation change using the DEMs exclusive of bedrock surfaces yielded slightly different results. The mean elevation change for this analysis was an increase of 63 m $\pm$ 144. Most of the elevation change occurred near the margins of the rocky outcrops, which were excluded from the elevation change analysis (Figure 33). The areas of highest elevation gain are shown as negative numbers because the elevation in these areas is higher in the 1951 DEM compared to the 2014 DEM, representing a net loss in elevation.

Based on continuing mass balance measurements collected on the Taku glacier, reasonable positive changes in elevation for this time period do not exceed 20 m (Pelto 2011). Areas of elevation loss within the same range as reasonable gains in elevation ($\geq$20 m) are present at the margins of the areas that experienced exaggerated mass loss (Figure 34). Areas that experienced elevation gain within 20 m follow a similar pattern and are proximate to the areas of mass loss (Figure 34).

Comparison of the DEM created from the 2014 GPS survey points showed similar results in terms of the locations of areas within reasonable amounts of elevation change. The mean amount of elevation change was an increase in elevation of 86 m $\pm$ 192.

Chapter 6 Discussion and Conclusions

This study offers a unique look at the effects of climate change on the Taku glacier system. Many of the variables analyzed in this study have been unquantified in either in situ studies or remote sensing analysis.

6.1 Glacier extent

Based on the analysis performed in this study, the Taku glacier experienced an overall decline in glacier surface as compared to bedrock in the accumulation zone and ablation zone, as well as in the bare ice in the accumulation zone. Most of the loss of glacier surface occurred in the accumulation zone as bedrock was exposed or snow surface transitioned to bare ice (Figure 21; Figure 9). It is possible that the high rate of melt surrounding the bedrock as compared to the rest of the accumulation zone is due to the positive feedback loop created by the interaction between the bedrock, solar input and the surrounding glacier surface. As discussed in previous sections, the low albedo and high heat capacity of the exposed bedrock promotes substantial melting of surrounding snow surfaces. Eventually, melting of the glacier adjacent to the rock occurs, creating a gap between the rock and the ice. This gap is part of a positive feedback loop that generates more melting as more rock is exposed (Paul et al. 2007). Increasing the area of exposed rock adjacent to a glacier can also increase the amount of windblown dust that accumulates on the glacier, which lowers albedo and can cause accelerated melting of the glacier (Bøggild, et al. 2010). A second positive feedback loop occurs once the snow surface has transitioned to bare ice and the associated albedo has been reduced. The lower albedo of bare ice compared to snow causes more heat to be retained and promotes further melting.

It is also possible that the glacier surfaces that experienced more substantial melting within the accumulation area received more solar input based on aspect. However, if aspect were the only factor contributing to increased melting, the observed trend of progressively larger areas of snow free ice and exposed bedrock within the accumulation zone from 1973 to 2015 would have been absent. Similarly, certain weather patterns such as wind might affect the amount of snow deposited in specific regions, but the areas of snow free ice and bedrock within the accumulation zone would be static rather than increasing in size.

Based on a visual comparison of the composite Landsat image and the reclassified raster representing glacier surface and bedrock, the method of using an unsupervised classification scheme to distinguish glacier surface from bedrock was effective and accurate. However, even though a composite image was used, it was not possible to distinguish between the bare ice of the ablation area and the bedrock surfaces of the accumulation zone. Experimentation with several different band combinations was performed, but none proved effective in distinguishing the bare ice of the ablation zone from bedrock in the accumulation zone. The method of separating the ablation area from the accumulation area and running the unsupervised classification separately proved effective and eliminated the need to use an excessive number of classes and perform tedious reclassification. The use of this method did necessitate the additional step of combining the glacier surface and bedrock values for the accumulation zone and ablation zone.

The Taku glacier is unique compared to other glaciers studied using remote sensing due in part to its exceptional size (Barcaza et al 2009; Pelto 2011). It is possible that its

large size and the presence of multiple facies, and gradients within those facies, on the glacier complicate the use of remote sensing to study glacier extent. Additionally, it is possible that airborne dust and debris accumulate at a higher rate on the main truck of the Taku glacier, compared to the accumulation zone, as the glacier narrows and is bounded on either side by bedrock (Bøggild et al. 2010). This accumulation of dust and debris might cause the reflectance of certain areas of the ablation zone to be very similar to the reflectance of exposed bedrock, making differentiation using satellite imagery difficult. This problem might be further compounded near the terminus of the glacier as glacier flow continues to move surface debris down glacier, thereby increasing the density of debris per area.

It is possible to remedy this problem by collecting in situ reflectance data characteristic of the accumulation zone, ablation zone and bedrock facies. These reflectance data should span the entire available reflective range of each facies and can subsequently be used to create a spectral library of the Taku glacier. This spectral library can then be used to inform satellite imagery analysis (Bøggild et al. 2010).

Traditional monitoring methods, including in situ measurements and remote sensing analysis do not quantify any transition in glacier facies that occurs at the margins of the glacier. Therefore, the exposure of bedrock and the transition of seasonal snow to snow free ice within the accumulation zone is largely underrepresented by these traditional monitoring methods. It is likely that the overall effect of climate change on alpine glaciers has been chronically underestimated and the situation is much more dire than previously considered.

6.2 Equilibrium Line Altitude and Accumulation Area Ratio

Delineation of the equilibrium line altitude from the composite satellite images proved efficient and accurate. The length of the equilibrium line was relatively insubstantial and made manual digitizing the most effective method in conjunction with creation of a composite image that enhanced contrast between the snow of the accumulation area and the bare ice of the ablation area.

From 1973-2015, Taku glacier experienced a considerable migration of the ELA up glacier, which coincides with a comparable reduction in AAR. The extended phase of positive mass balance from 1946-1988 of the Taku glacier, as well as its exceptionally large size, has resulted in an uncommonly high AAR for a non-calving glacier. The AAR of 0.86 during 1973 puts the glacier well within positive mass balance. The lowest AAR value recorded based on the above analysis is 0.67 in 2015. The equilibrium AAR value for the Taku glacier has been established as 0.67 and the presence of this value in 2015 likely heralds a cessation of advancement and the onset of retreat and thinning (Pelto 2011).

Analysis of the α_d associated with each Landsat scene yield similar results. The α_d value for Taku glacier drops from 0.86 in 1973 to zero in 2015; value of zero indicates no advancement. α_d is thought to be a more immediate indicator of response to shifts in the climatic regime and the Taku glacier is likely to slip past zero into the realm of negative α_d values, which will indicate that the glacier is in retreat (Dyurgerov et al. 2009).

When winter accumulation cannot persist through summer melting because of a reduction in precipitation, an increase in summer temperatures, or an increase in the

length of the ablation season, the AAR is reduced and the glacier is no longer in equilibrium. If the AAR is reduced, there is typically a corresponding migration of the ELA to a higher elevation, often associated with glacier thinning and terminus retreat (Barcaza et al. 2009; Cheung-Wai et al. 2009; Dyurgerov et al. 2009). The unique hypsometry of the Taku glacier makes it particularly susceptible to changes in temperature resulting in a significant migration of the ELA up glacier (Figure 11).

Due to the relative paucity of mass at the terminus of the glacier, the Taku glacier is typically slow to respond to initial changes in climate. However, a considerable percentage of the mass of the Taku glacier lies between 1200 and 1600 m elevation. Once temperatures have continued to warm and the ELA migrates above 1200 m, any successive migration up glacier of the ELA will convert a significant area of the glacier to ablation zone (Pelto et al. 2008; Pelto 2011). Once this surface no longer retains seasonal snow, the lower albedo characteristic of the ablation zone will create a positive feedback loop, which will induce further melting (Paul et al. 2007). Further monitoring is needed to determine if the observable trend of migration of the ELA up glacier and reduction in AAR will continue as predicted on the Taku Glacier.

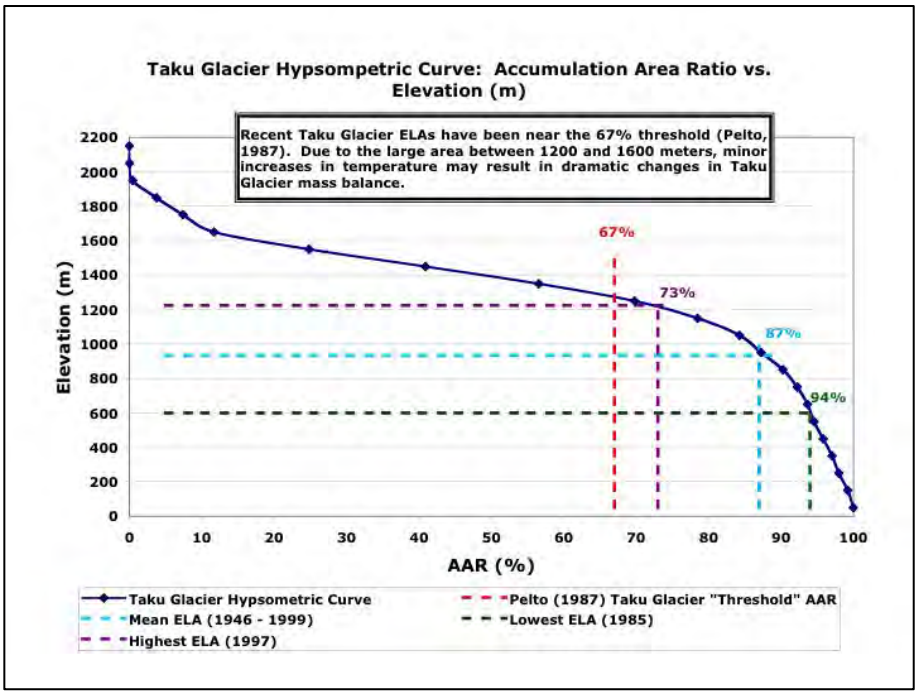

Figure 11 Hypsometric curve for the Taku Glacier.

6.3 Elevation change on the Taku glacier from 1951 to 2015

The Taku glacier has experienced significantly positive mass balance from 1946-1988 with a mean annual balance of 0.42 m a^{-1} (Figure 12). A mean annual balance of this magnitude amounts to a total glacier surface thickening of 17.5 m w.e., equivalent to 20 m in gross ice thickness. From 1989-2006, the average annual balance turned slightly negative to -0.14 m a^{-1} (Figure 12). This negative average annual balance is equivalent to 2.7 m w.e. loss, analogous to a loss of three meters of glacier surface. Given these gains and losses to the glacier surface, the Taku glacier has experienced a total gain of 17 m in glacier thickness from 1946-2006 (Pelto et al. 2008). These data are extrapolated from mass balance surveys conducted by JIRP (Pelto et al. 2008; Larsen et al. 2006).

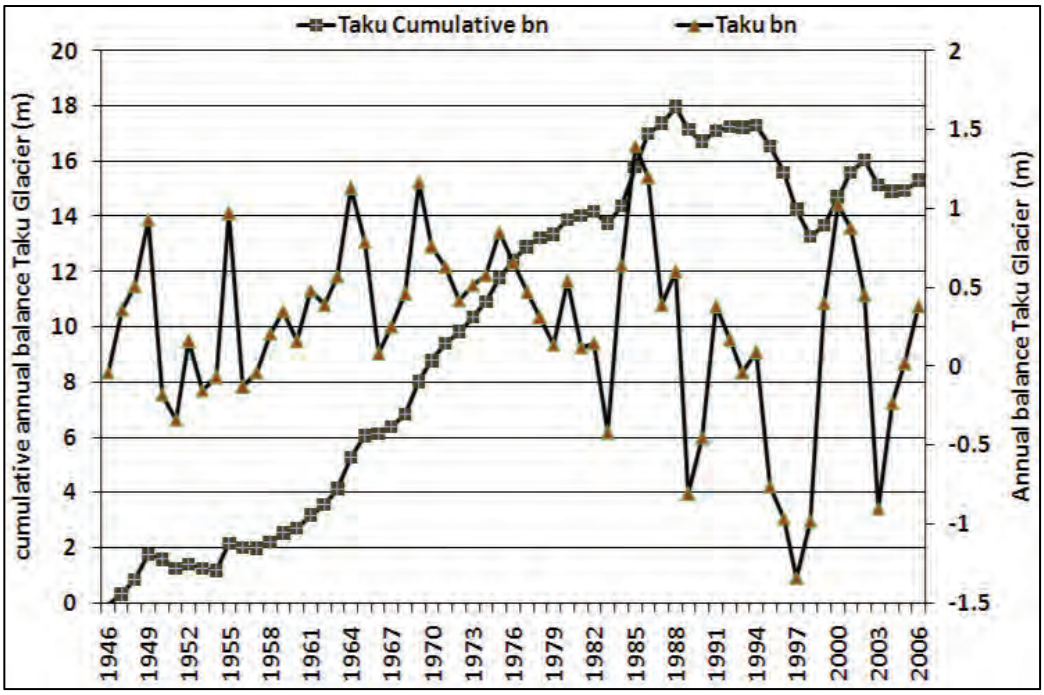

Figure 12 Annual and cumulative balance of the Taku Glacier from 1946-2006 (Pelto et al. 2008).

Despite the overall trend of positive mass balance from 1951 to 2015, it was hypothesized before the initiation of this study that specific areas of the glacier might be characterized by elevation loss as temperatures rose and precipitation decreased, causing changes to the local climatic regime. Comparison of the DEM generated from the 1951 historical topographic map and the 2014 USGS DEM generate inconclusive results. Analysis using the method of DEM comparison is complicated because only the glacier surfaces were digitized on the historical topographic map due to the poor resolution of the historical topographic map. As a result, comparison of the DEMs shows considerably inflated elevation increase in these areas. In an effort to alleviate this problem, the non-digitized areas were excluded from both DEMs, but this did not improve the accuracy of the

elevation change analysis. Based on these shortcomings it is difficult to draw any substantial conclusions from the DEM comparison. It is especially suspicious that areas that lost an amount of mass within a reasonable threshold and areas that gained an amount of mass within a reasonable threshold are directly adjacent to each other (Figure 34). Due to the inconclusiveness of the results of the DEM comparison, it is not possible to establish any perceptible trend of elevation gain or loss across the Taku glacier during this time period.

6.4 Further Research

Continued monitoring of the Taku glacier will determine if the trends observed in this study will persist into future years. As additional Landsat scenes taken at the end of the ablation period become available, they should be analyzed using the same methods described above. Development of a spectral library using in situ reflectance data might aid in the classification of glacier facies from remote sensing images. In situ reflectance data would need to be collected within each glacier facies and represent as close to the full spectrum of the reflectance within that facies as possible. These data could then be used to inform the classification of the glacier surface in remote sensing images. If, based on in situ analysis, the ablation area is known to exist within a specific range of spectral reflectance, then areas determined to be within this range using remotely sensed imagery can be classified as ablation zone facies.

6.5 Final Conclusions

The use of remote sensing images to quantify changes in glacier extent, ELA and AAR, and elevation has proved effective and accurate. This study shows that using the combination of glacier extent, ELA and AAR as well as elevation change offers a comprehensive look at a glacier's response to climate change through time. The results of the glacier surface area change analysis show that traditional in situ monitoring as well as remote sensing monitoring of AAR without the consideration of increasingly prevalent transitions from seasonal snow to snow free ice in the accumulation zone grossly underestimate the effects of climate change on alpine glaciers.

The initiation of comprehensive analysis using remote sensing in addition to in situ monitoring is especially crucial given the Taku glacier's long history of advancement and recent changes in terminus dynamics (Molina 2006). The use of remote sensing to study large and previously advancing glaciers in North America has been limited. This study demonstrates that drawing conclusions from in situ measurements alone can lead to grossly underestimating the amount of change that is happening across a glacier in response to climate change. Remote sensing analysis is valuable in addition to or in place of in situ measurements.

The Taku glacier has experienced a long history of advancement and has been typically slow to respond to changes in temperature and precipitation. The results of this study, which find a reduction in total glacier surface, the ELA migrating consistently up glacier, and a reduction in AAR from 1973-2015, likely indicate a cessation in advancement of this glacier. Given that the Taku glacier is typically slow to respond to changes in climate, but is demonstrating substantial changes in previously unmeasured metrics, it is possible

that surrounding glaciers with more typical responds to changes in climate have already undergone dramatic changes that have been unnoticed and unquantified by traditional monitoring methods.

Unfortunately, the analysis of elevation change did not yield conclusive results. It is possible that limiting the analysis period to more recent years more similar to the timeline used for the glacier extent and ELA analysis (1973-2915) might produce more conclusive results due to the elimination of the need to digitize a historical topographic map. It is important to understand if down wasting of the glacier is occurring at the glacier margins. The dangerous conditions present at the margins of a glacier make remote sensing the only viable options for monitoring. However, it is possible that the surface area change analysis effectively captures the downwasting at the margins of the glacier as snow transitions to snow free ice and analysis of elevation change in these same areas might be redundant.

REFERENCES

Arendt, Anthony A. 2006. Volume changes of Alaska glaciers: contributions to rising sea level and links to changing climate. (Doctoral dissertation) University of Alaska Fairbanks.

Bamber, Jonathan L. and Andres Rivera. 2007. A review of remote sensing methods for glacier mass balance determination. Global and Planetary Change 59, no. 1-2 (October): 138-148.

Baolin, Li, Zhang Yichi, and Zhou Chenghu. 2004. Remote sensing detection of glacier changes in Tianshan Mountains for the past 40 years. Journal of Geographical Sciences 14, no. 3 (May): 296-302.

Barcaza, Gonzalo, Masamu Aniya, Takane Matsumoto, and Tatsuto Aoki. 2009. Satellite-derived equilibrium lines in Northern Patagonia Icefield, Chile, and their implications to glacier vatiations. Artic, Antarctic, and Alpine Research 41, no. 2 (May): 174-182.

Berthier, Etienne, Yves Arnaud, D. Baratoux, C. Vincent, and F. Rémy. Recent rapid thinning of the "Mer de Glace" glacier derived from satellite optical images. Geophysical Research Letters 31, no. 1 (September): L17401.

Berthier, Etienne, Yves Arnaud, Rajesh Kumar, Sarfaraz Ahmad, Patrick Wagnon, and Pierre Chevallier. 2006. Remote sensing estimates of glacier mass balances in the Himachal Pradesh (Western Himalaya, India). Remote Sensing of Environment 108, no. 1 (November): 327-338.

Bøggild, C.E., R.E. Brandt, K.J. Brown and S.G. Warren. 2010. The ablation zone in northeast Greenland: ice types, albedos and impurities. Journal of Glaciology 56, no. 195: 101-113.

Chander, Gyanesh, Brain L. Markham and Dennis L. Helder. 2009. Summary of current radiometric calibration coefficients for Landsat MSS, TM, ETM+, and EO-1 ALI sensors. Remote Sensing of Environment, no. 113 (January): 893-903.

Cheung-Wai Chan, Jonathan, Jeremy Van Ophem, and Philippe Huybrechts. 2009. Estimation of accumulation area ratio of a glacier from multi-temporal satellite images using spectral unmixing. Geoscience and Remote Sensing Symposium (July): 606-609.

Church, John A. and Neil J. White. 2006. A 20th century acceleration in global seal-level rise. Geophysical Research Letters 33, no. 1 (January): L01602.

Dyurgerov, Mark, Mark F. Meier, and David B. Bahr. 2009. A new index of glacier area change: a tool for glacier monitoring. Journal of Glaciology 55, no. 192 (May): 710-716.

Echelmeyer, K.A., M. Nolan, R. Motyka, and D. Trabant. 1995. Ice thickness measurements of the Taku Glacier, Alaksa, USA and their relevance to its recent behavior. Journal of Glaciology 41 no. 139 (April): 541-552.

Echelmeyer, K.A., W. D. Harrison, C.F. Larsen, J. Sapiano, J.E. Mitchell, J. DeMallie, B. Rabus, G. Adalgeirsdóttir, and L. Sombardier. 1996. Airborne surface profiling of glaciers: a case-study in Alaska. Journal of Glaciology 42 no. 142 (April): 538-547.

Haq, M Anul, Kamal Jain, and K.P.R. Menon. 2012. Change Monitoring of Gangotri Glacier using Remote Sensing. International Journal of Soft Computing and Engineering 1, no. 6 (January): 259-261.

Kargel, Jeffery S., Michael J. Abrams, Michael P. Bishop, Andrew Bush, Gordon Hamilton, Hester Jiskoot, Andreas Kääb, Hugh H. Kieffer, Ella M. Lee, Frank Paul, Frank Rau, Bruce Raup, John F. Shroder, Deborah Soltesz, David Stainforth, Leigh Stearns, Rick Wessels. 2005. Multispectral imaging contributions to global land ice measurements from space. Remote Sensing of Environment 99, no. 1 (July): 187-219.

Karpilo, Ronald D. 2009. Glacier monitoring techniques. The Geological Society of America.

Khalsa, Siri, J.S., Mark B. Dyurgerov, Tatiana Khromova, Bruce H. Raup, and Roger G. Barry. 2004. Space-based mapping of glacier changes using ASTER and GIS tools. IEEE Transactions on Geoscience and Remote Sensing 42, no. 10 (October): 2177-2183.

Larsen, Christopher F., Roman J. Motyka, Anthony A. Arendt, Keith A. Echelmeyer, and Paul E. Geissler. 2006. Glacier changes in southeast Alaska and northwest British Columbia and contribution to sea level rise. Journal of Geophysical Research 112, no. 1 (June): F01007

Leonard, Katherine C. and Andrew G Fountain. 2003. Map-based methods for estimating glacier equilibrium-line altitudes. Journal of Glaciology 49, no. 166 (March): 329-336.

Li, Peng, Chuang Shi, Zhenhong Li, Jan-Peter Muller, Jane Drummond, Xiuyang Li, Tao Li, Yingbind Li, and Jingnan Liu. 2013. Evaluation of ASTER GDEM using GPS benchmarks and SRTM in China. International Journal of Remote Sensing 35, no. 5 (November): 1744-1771.

Liang, Shunlin, Hongliang Fang, Jeffrey T. Morisette, Mingzhen Chen, Chad J. Shuey, Carles L. Walthall, and Craig S.T. Daughtry. 2002. Atmospheric correction of Landsat ETM+ land surface imagery: II Validation and Applications. IEEE Transactions on Geoscience and Remote Sensing.

Meier, Mark F., Mark B Dyurgerov, and Gregory J. McCabe. 2003. The health of glaciers: recent changes in glacier regime. Climatic Change 59, no. 1 (July): 123-135.

Molnia, Bruce F. 2006. Late nineteenth to early twenty-first century behavior of Alaskan glaciers as indicators of changing regional climate. Global and Planetary Change 56, (October): 23-56.

Motyka, R.oman J., Shad O'Neel, Cathy L. Conner, Keith A. Echelmeyer. 2003. Twentieth century thinning of Mendenhall Glacier, Alaska, and its relationship to climate, lake calving, and glacier run-off. Global and Planetary Change 35, no. 1-2 (January): 93-112.

National Aeronautics and Space Administration. 2011. Landsat 7 Science Data Users Handbook.

Neal, Edward G., Eran Hood, and Kathy Smikrud. 2010. Contribution of glacier runoff to freshwater discharge into the Gulf of Alaska. Geophysical Research Letters 37, no. 1 (January): L06404.

Pandey, Arvind C., Swagata Ghosh, M.S. Nathawat, and Reet K. Tiwari. 2012. Area Change and Thickness Variation over Pensilungpa Glacier (J&K) using Remote Sensing. Journal of Indian Society of Remote Sensing 40, no. 2 (June): 245-255.

Paul, Frank, Andreas Kääb, and Wilfried Haeberli. 2007. Recent glacier changes in the Alps observed by satellite: Consequences for future monitoring strategies. Global and Planetary Change 56, no. 1-2 (March): 111-122.

Peduzzi, P., Herold, C. and Silverio, W. 2009. Assessing high altitude glacier thickness, volume and area changes using field, GIS and remote sensing techniques: the case of Nevado Coropuna (Peru). The Cryosphere 4, (October): 313-323.

Pelto, Mauri S., Maynard M. Miller, G.W. Adema, Matthew J. Beetle, Scott R. McGee, Kenneth F. Sprenke, and Martin Lang. 2008. The equilibrium flow and mass balance of the Taku Glacier, Alaska 1950-2006. The Cyrosphere 2, no. 3 (November): 275-298.

Pellikka, Petri E. and Gareth W. Rees. 2010. Remote sensing of glaciers. AK Leiden, The Netherlands: CRC Press/Balkema.

Post, Austin and Edward R. LaChapelle. 2000. Glacier Ice. University of Washington Press.

Rabatel, A., A. Letréguilly, J.P Dedieu, and N. Eckert. 2013. Changes in glacier equilibrium-line altitude in the western Alps from 1984 to 2010: evaluation by remote sensing and modeling of the morpho-topographic and climate controls. The Cryosphere 7, no.1 (September): 1455-1471.

Raup, Bruce, Andreas Kääb, Jeffery S. Kargel, Michael P. Bishop, Gordon Hamilton, Ella Lee, Frank Paul, Frank Rau, Deborah Soltesz, Siri Jodha Singh Khalsa, Matthew Beedle, and Christopher Helm. 2007. Remote sensing and GIS technology in the Global Land Ice Measurements from Space (GLIMS) project. Computers and Geosciences 33, no. 1 (January): 104-125.

Truffer, Martin, Roman J. Motyka, Michael Hekkers, Ian M. Howat, Matt A. King. 2009. Terminus dynamics at an advancing glacier: Taku Glacier, Alaska. Journal of Glaciology 55, no. 194 (October): 1052-1060.

Zemp, M., E. Thibert, M. Huss, D. Stumm, C. Rolstad Denby, C. Nuth, S.U. Nussbaumer, G. Moholdt, A. Mercer, C. Mayer, P.C. Joerg, P. Jansson, B. Hynek, A. Fischer, H. Escher-Vetter, H. Elvehøy, and L.M. Andreassen. 2013. Reanalyzing glacier mass balance measurement series. The Cryosphere 7, no. 1 (August): 1227-1245.

Appendix A: Modifications to the Global Land Ice Measurements from Space Outline of the Taku Glacier

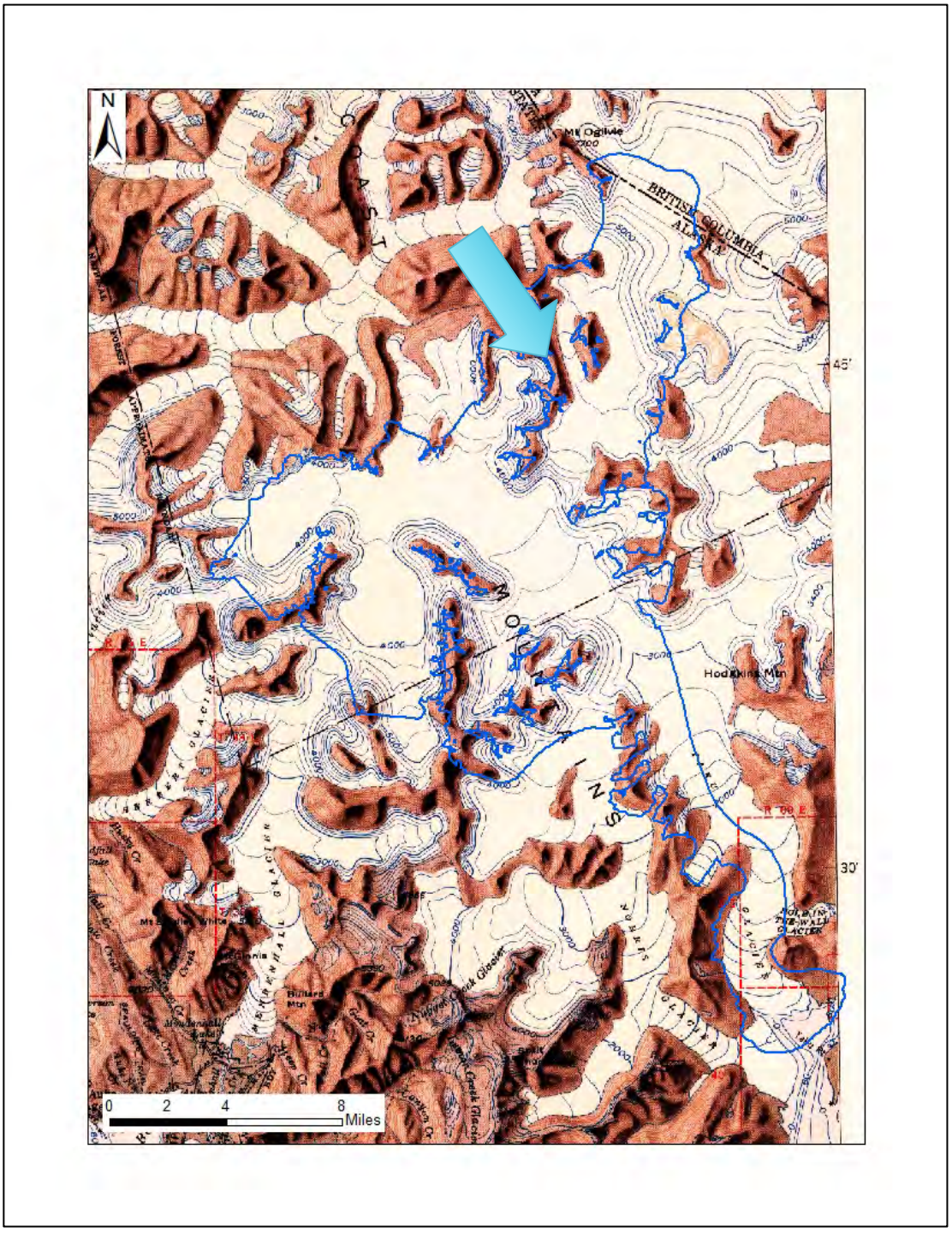

Figure 13 Map showing GLIMS Taku glacier polygon outlined in blue. Blue arrow is identifying general area where glacier flow is away from the Taku terminus.

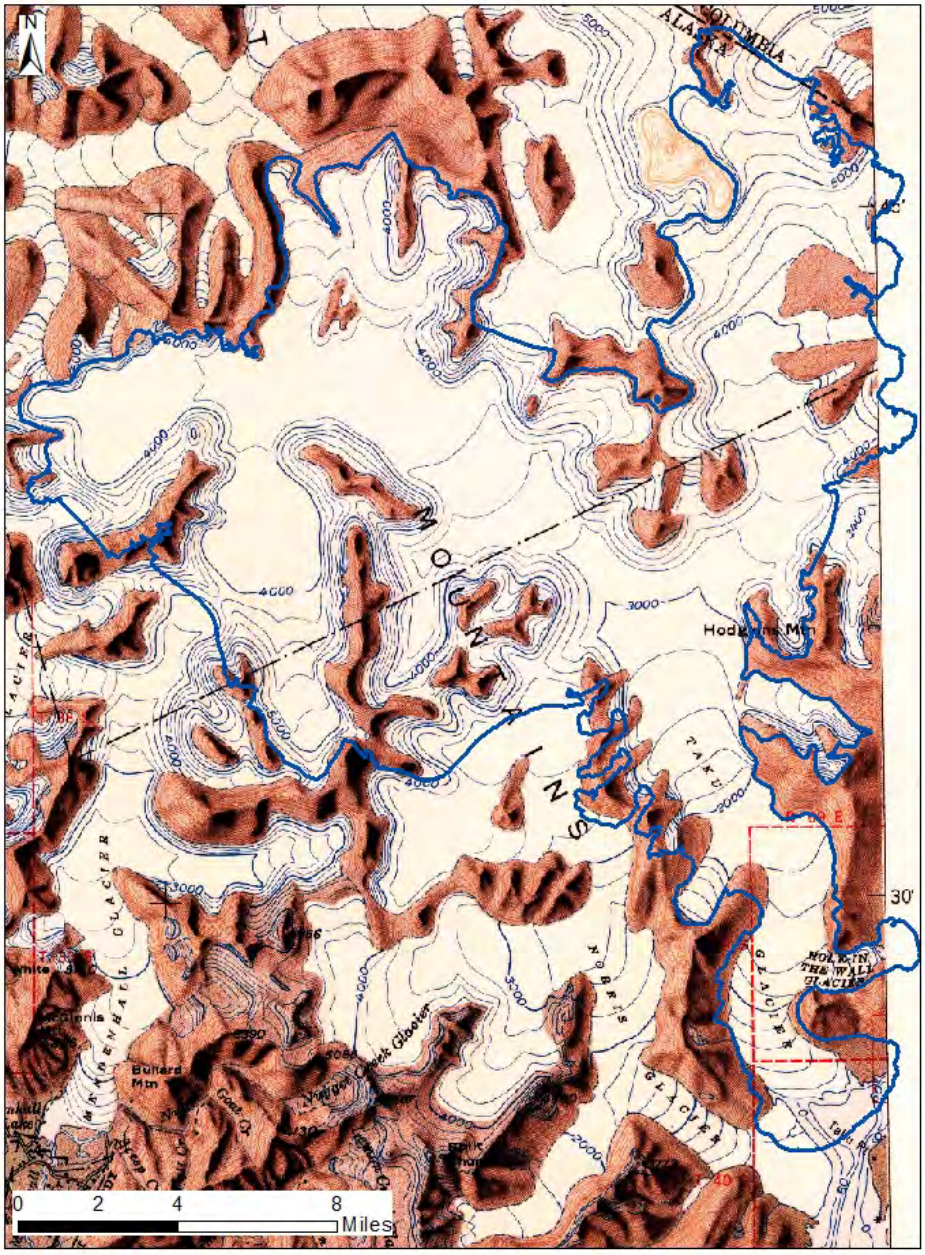

Figure 14 Complete Taku glacier polygon used in this study.

Appendix B: Images associated with delineation of ELA and total glacier surface area methods.

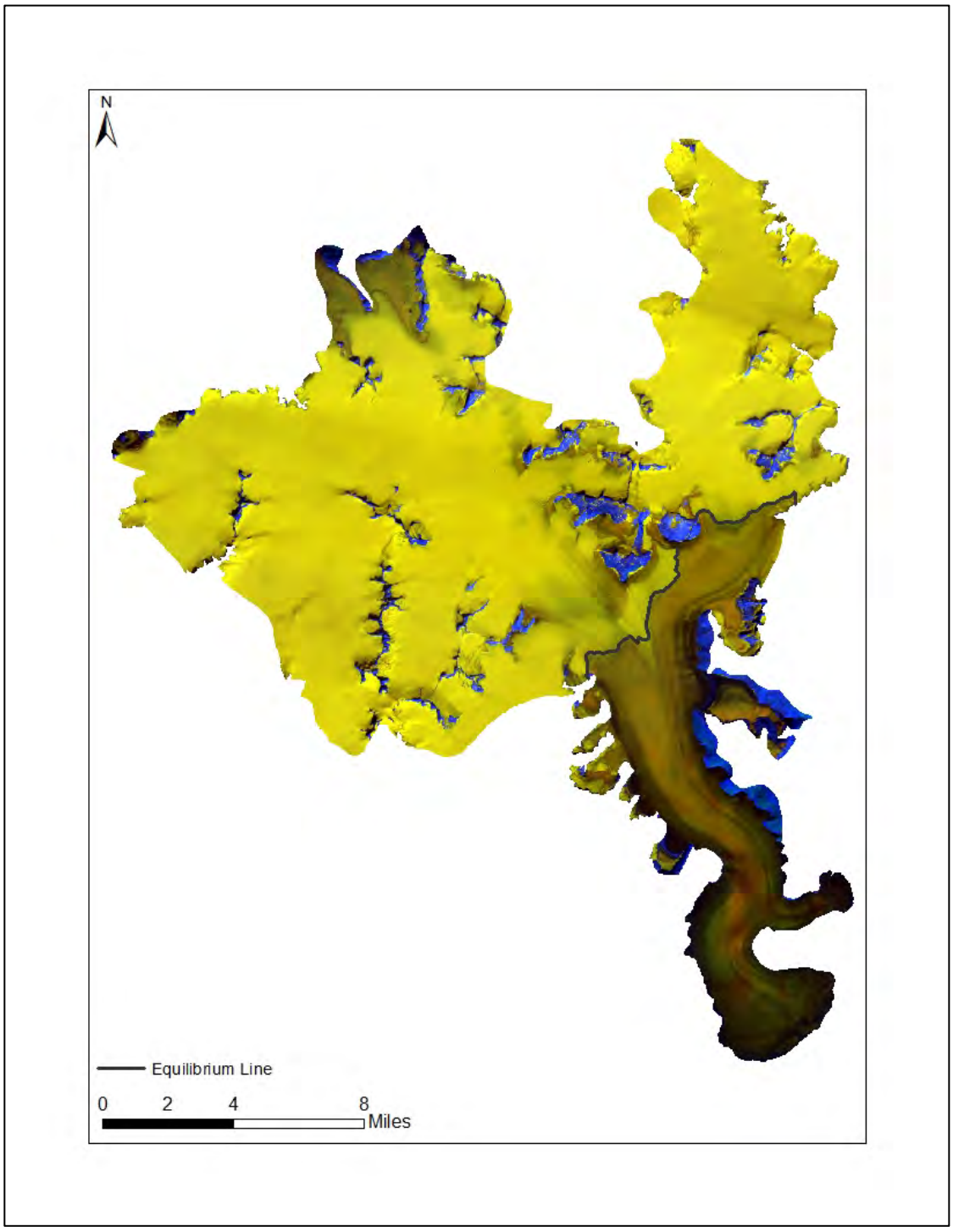

Figure 15 Composite image of the 2015 Landsat 8 scene including band 3 (green), band 5 (near-infrared), and band 6 (Short-wave infrared).

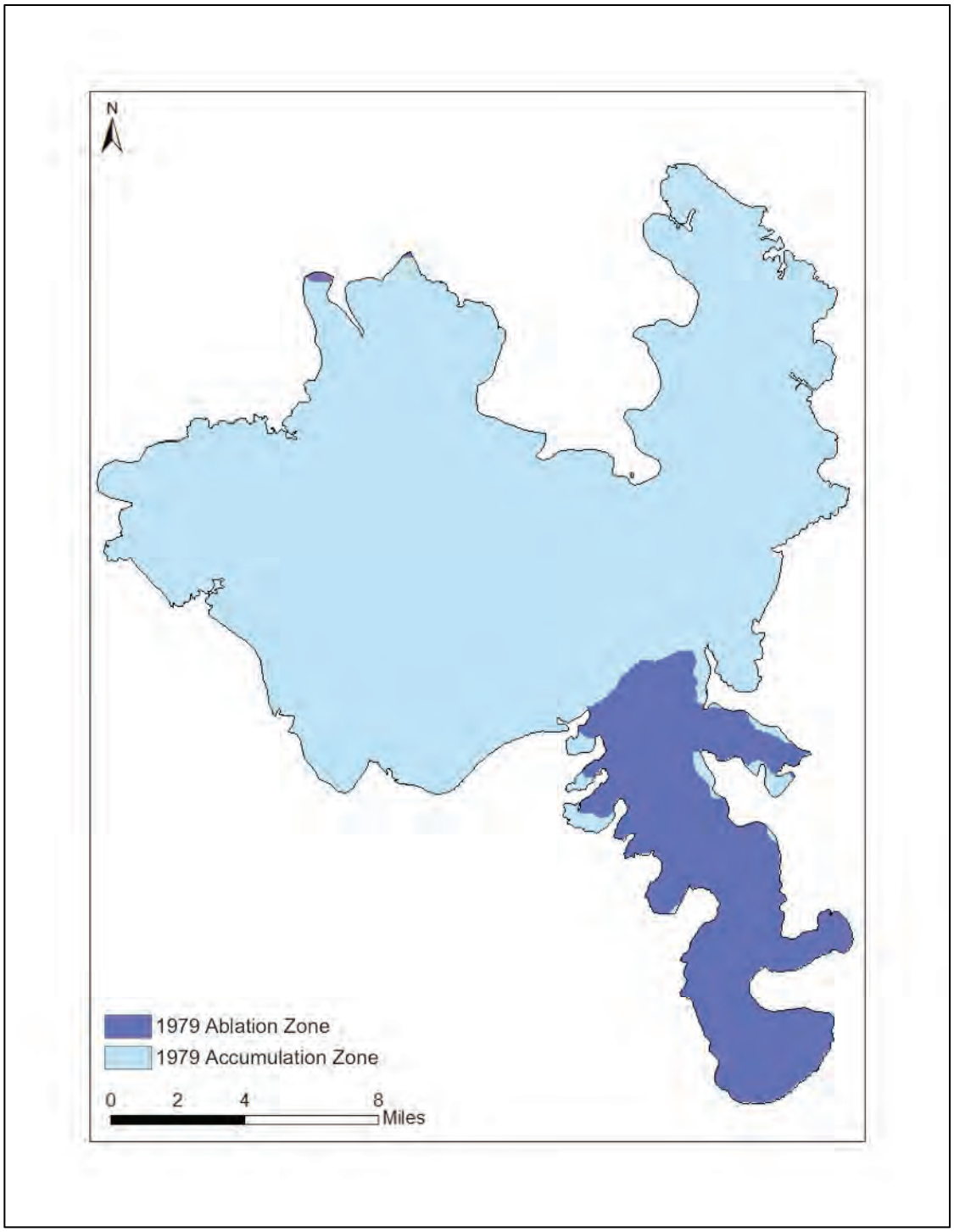

Figure 16 Map showing ablation zone and accumulation zone based on the ELA of the 1979 Landsat scene.

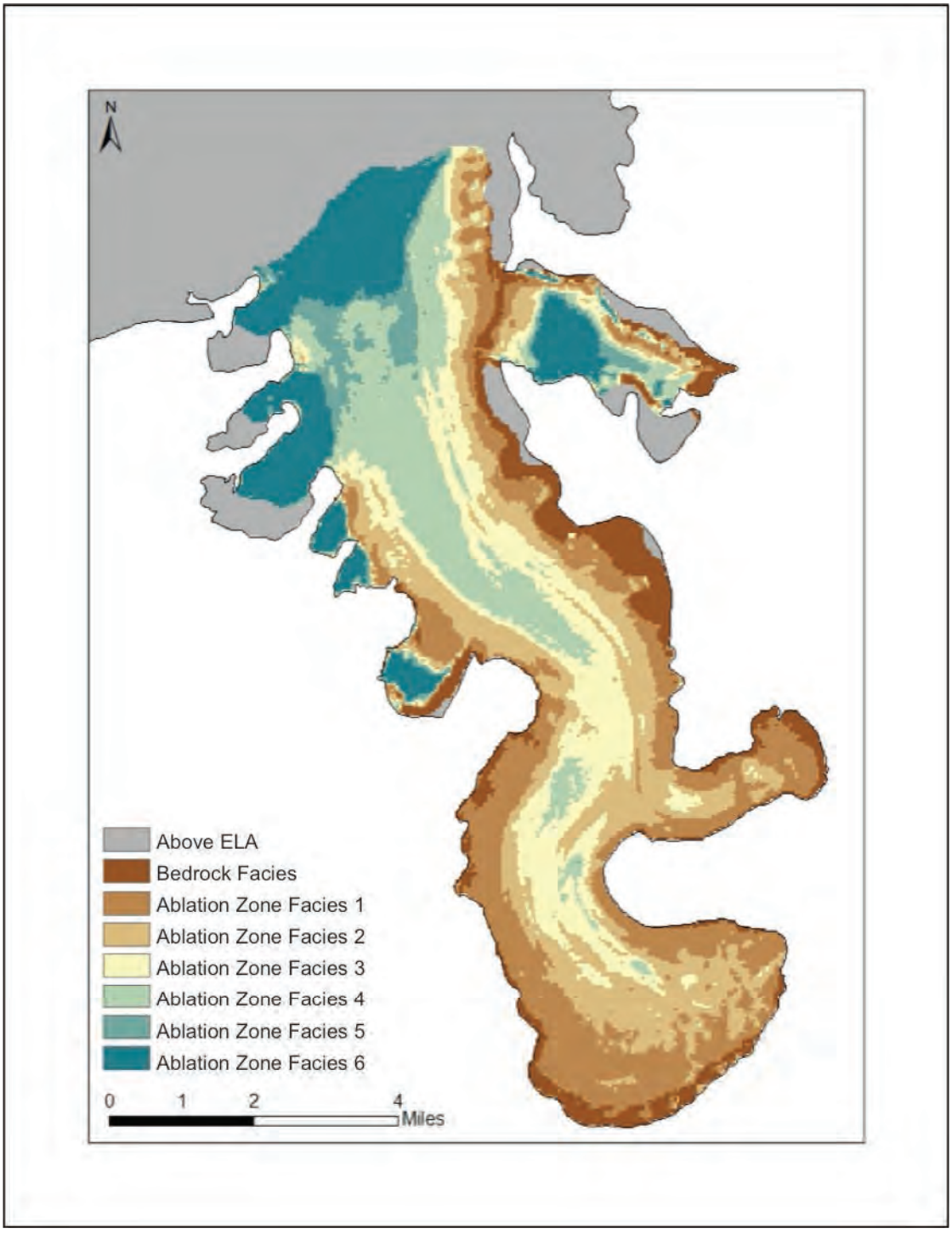

Figure 17 Map showing eight classes generated by the unsupervised classification for the 1979 scene.

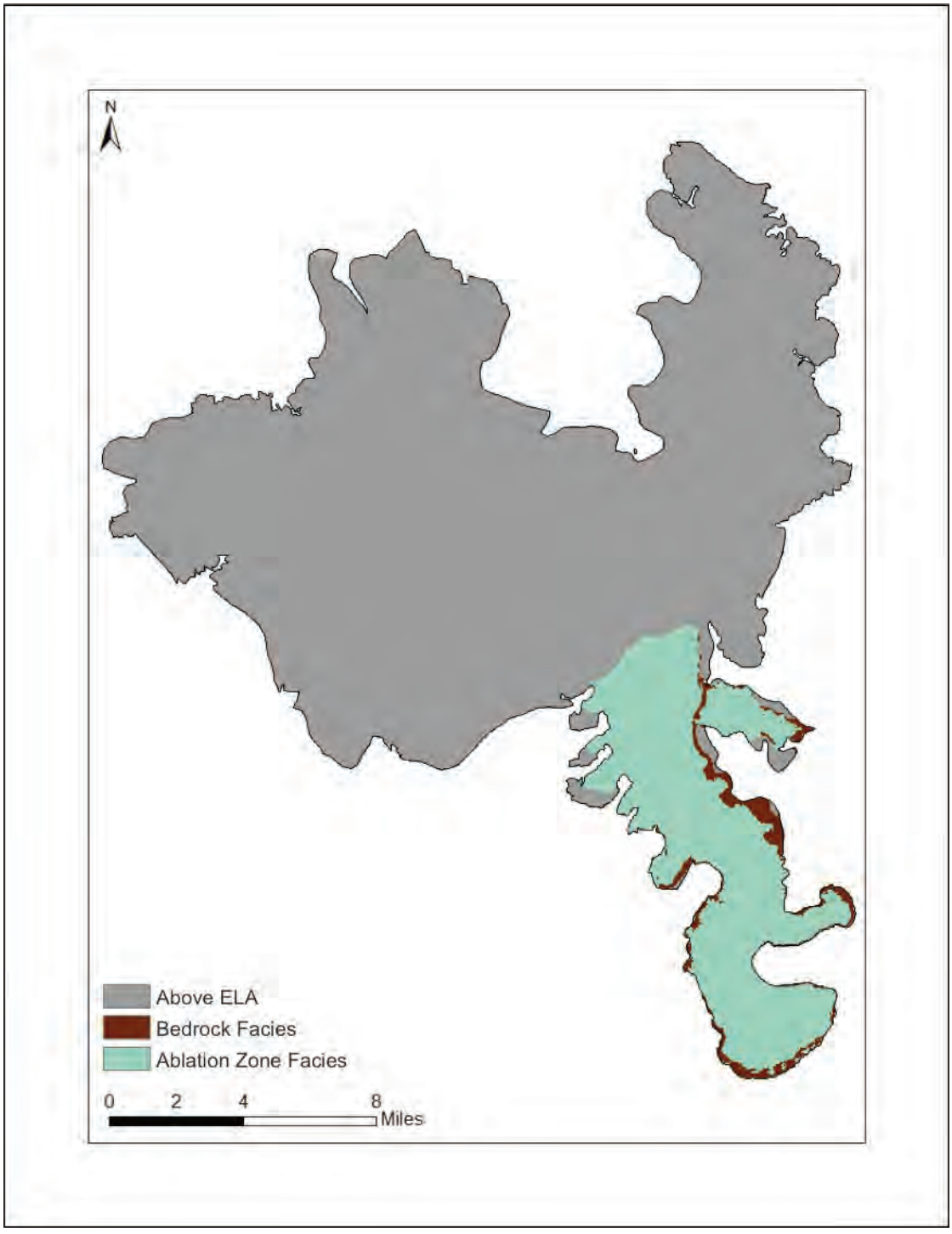

Figure 18 Map showing glacier surface and surrounding bedrock in the ablation zone of the 1979 scene.

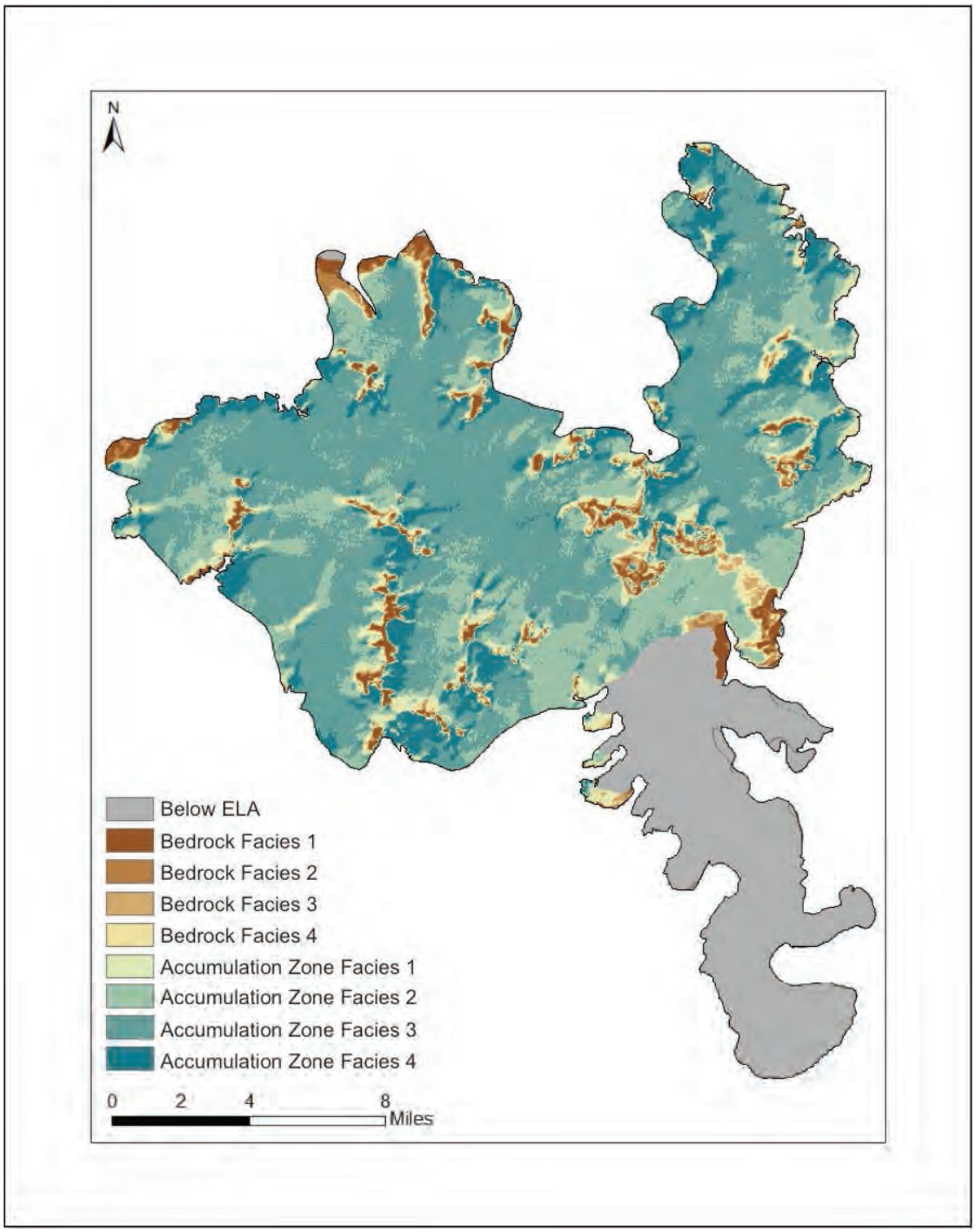

Figure 19 Map showing eight classes generated by the unsupervised classification for the accumulation area for the 1979 scene.

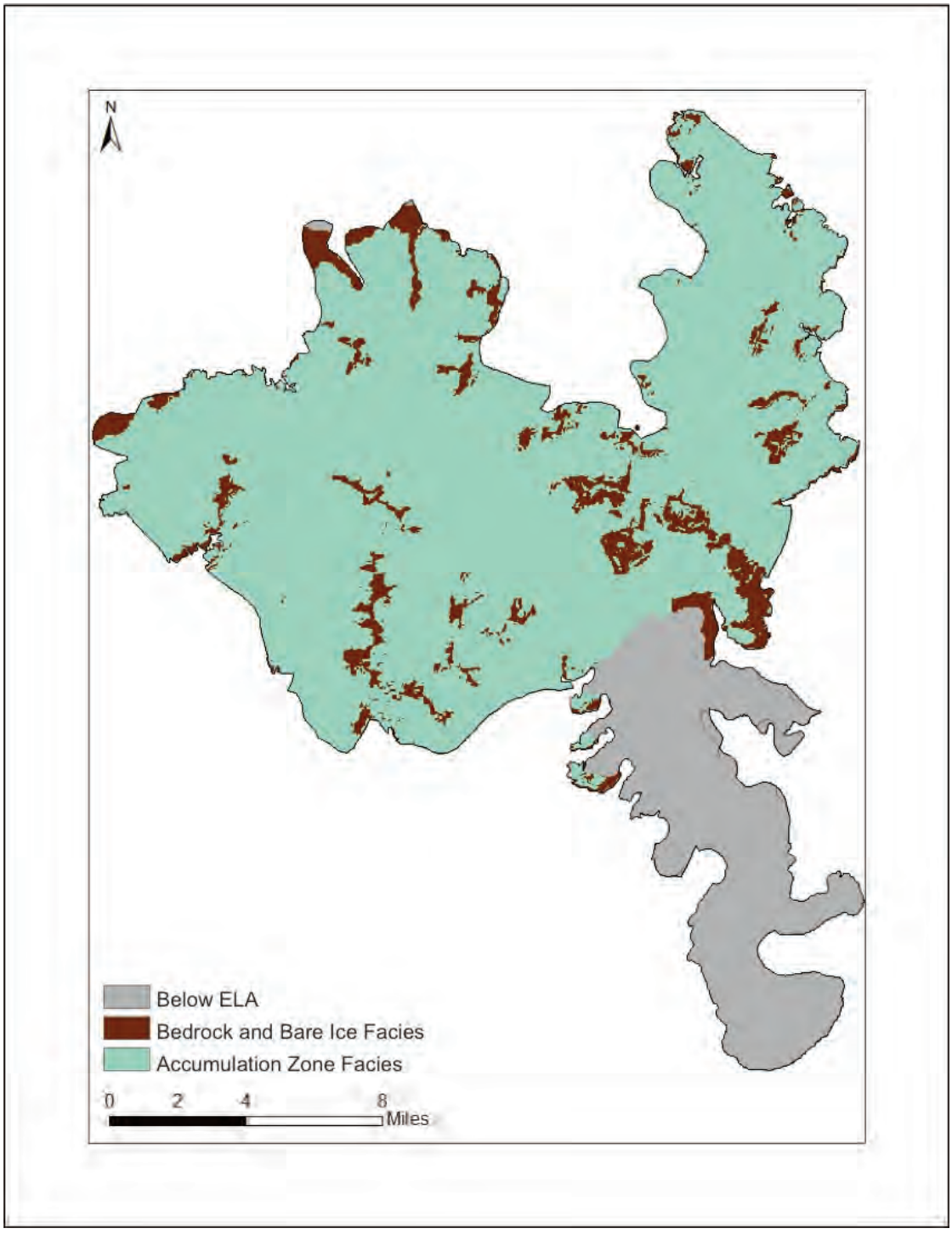

Figure 20 Map showing glacier surface and surrounding bedrock in the accumulation zone of the 1973 scene.

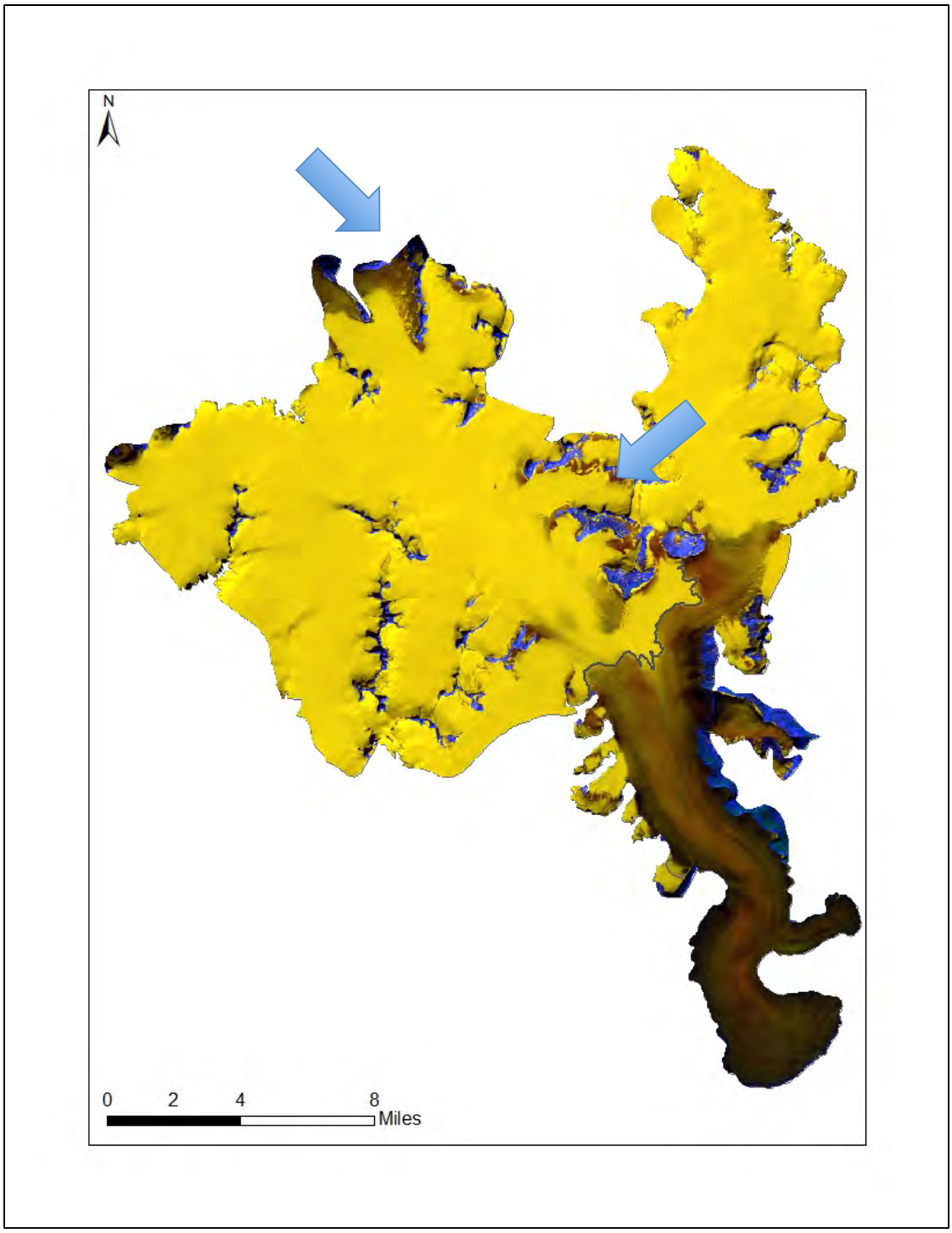

Figure 21 Composite image of 2004 Landsat scene accumulation zone. Bare ice is indicated by blue arrows.

Appendix C: Images associated with digitization of historical topographic map methods and elevation change analysis.

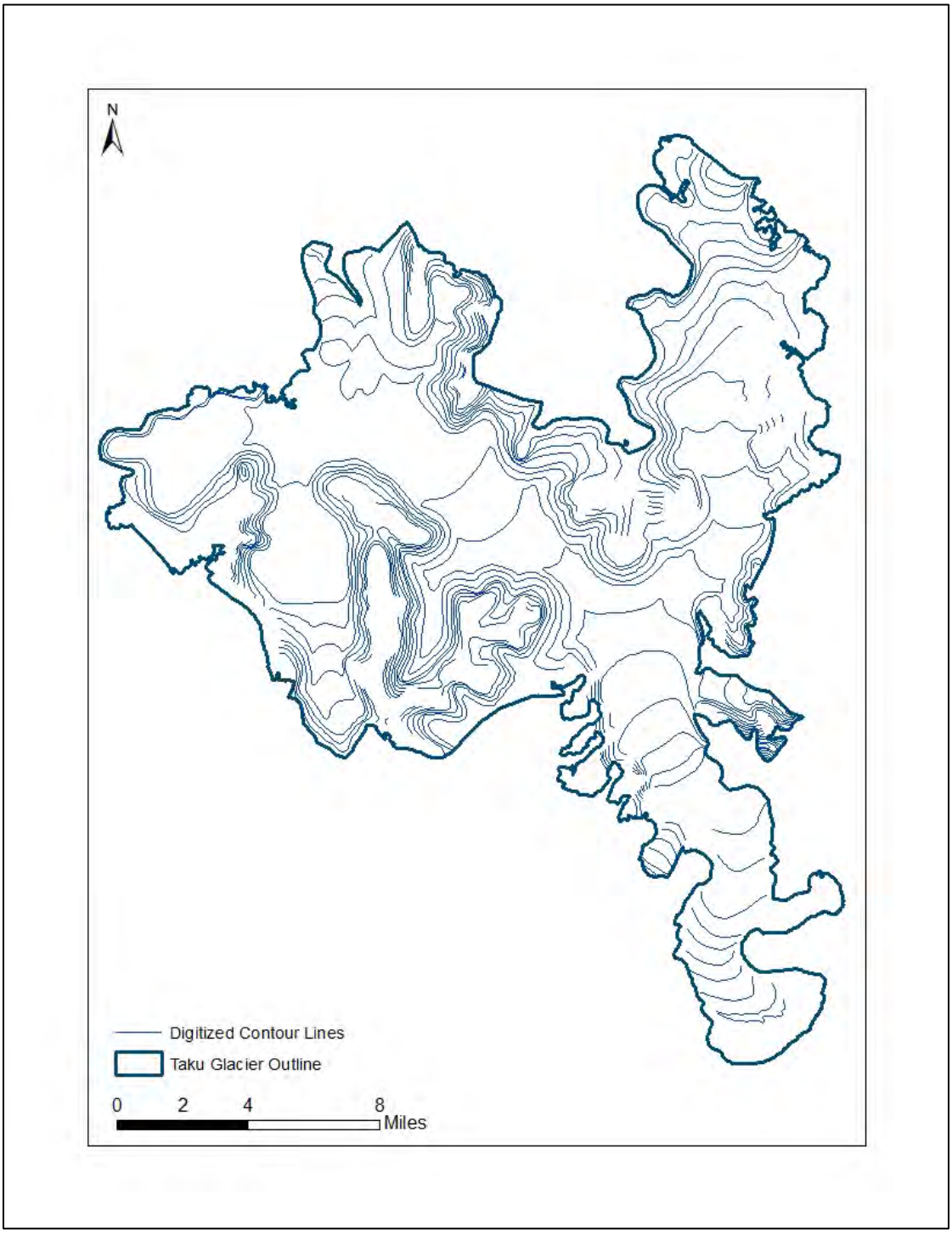

Figure 22 Map showing digitized contour lines.

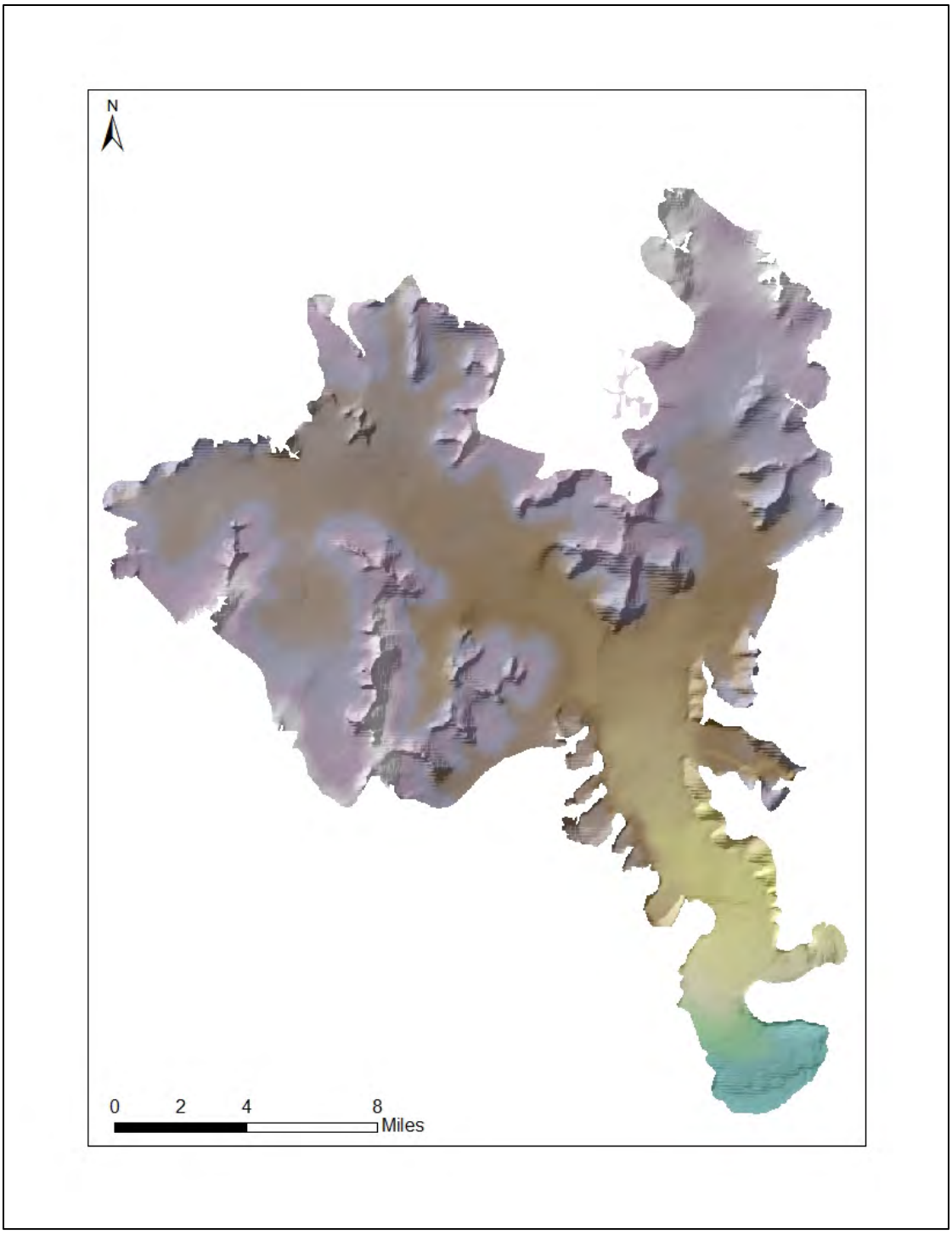

Figure 23 Map showing DEM created from the historical topographic map. The hillshade was created from the USGS DEM.

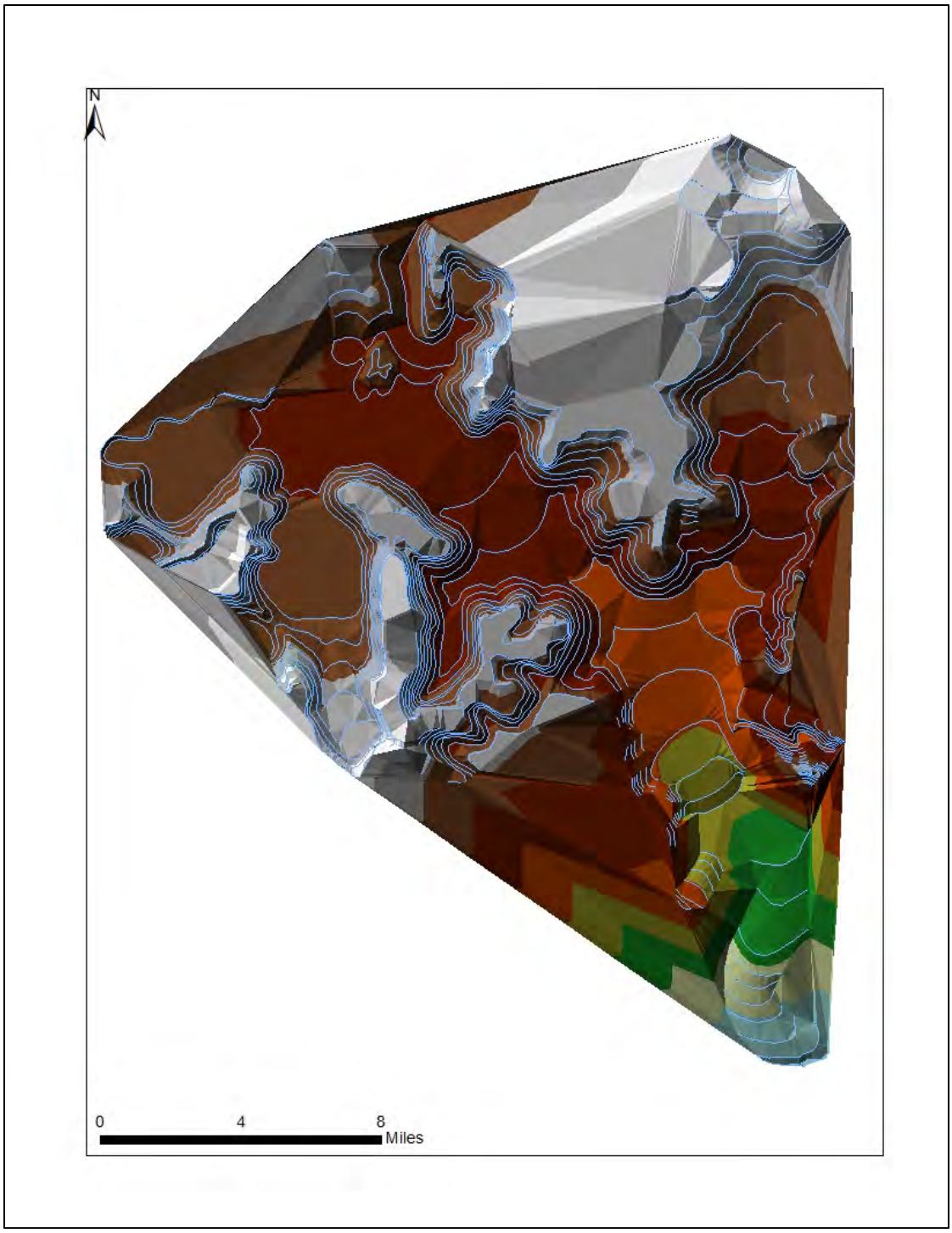

Figure 24 TIN generated from 1951 digitized contour lines.

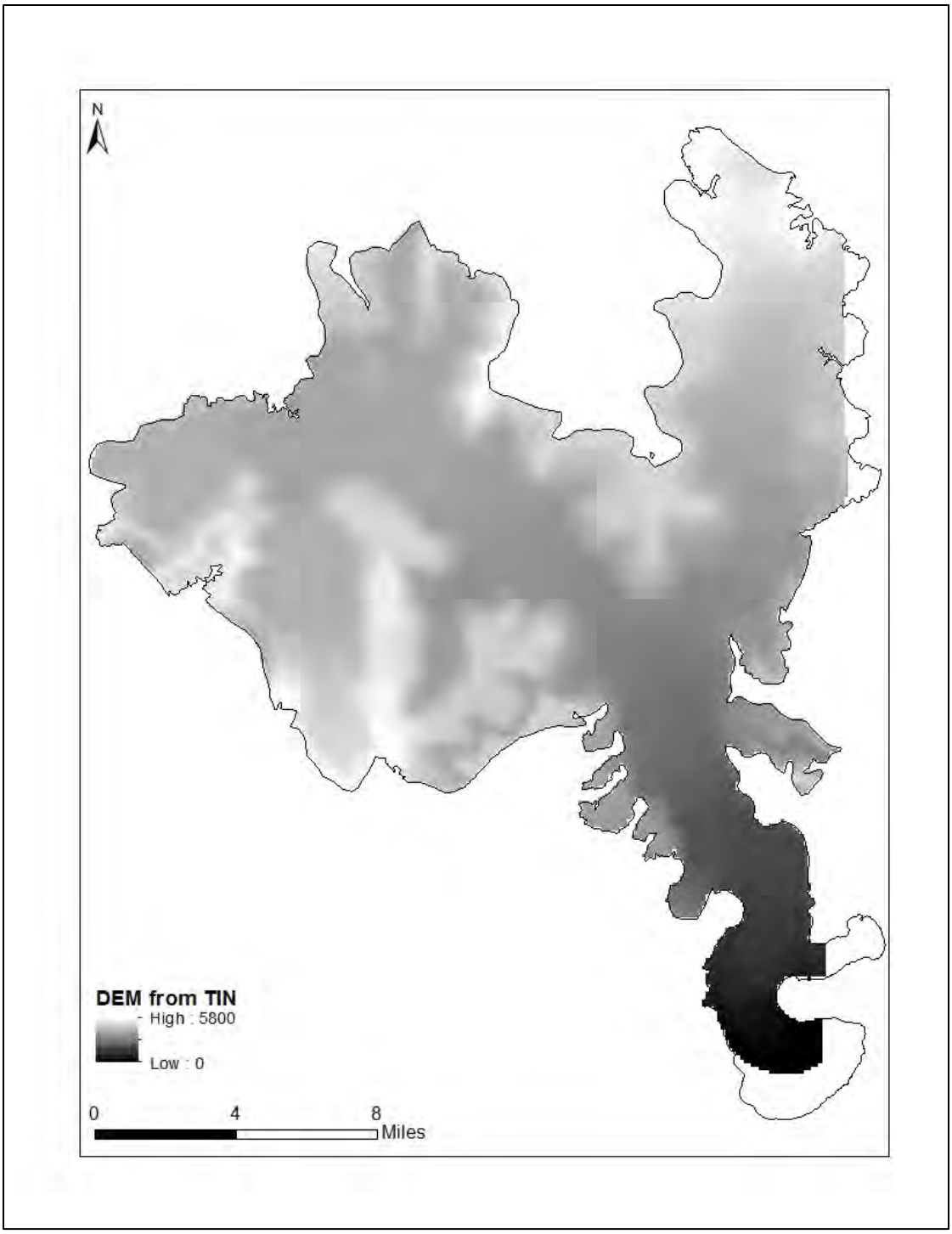

Figure 25 DEM (m) created from TIN.

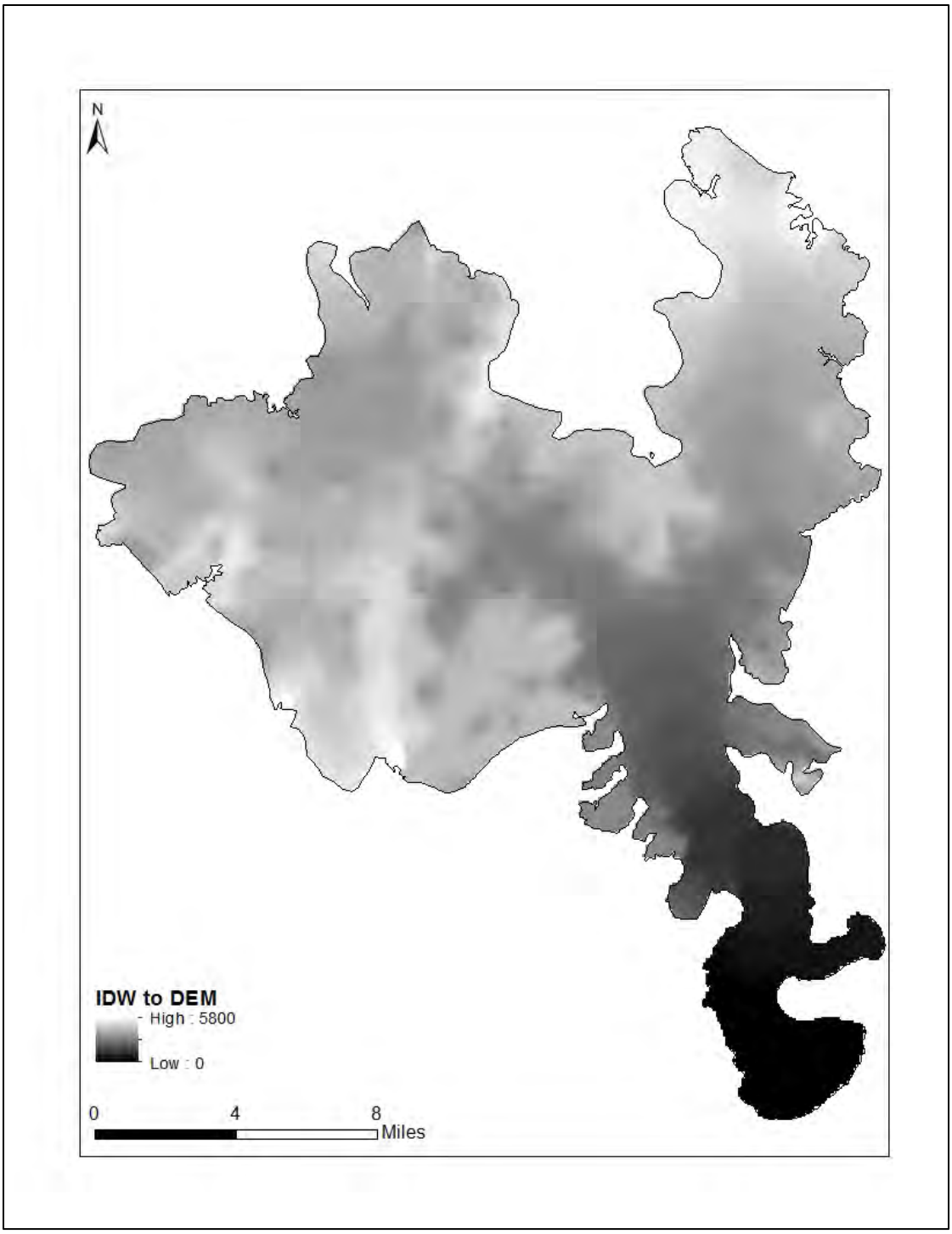

Figure 26 DEM (m) generated using IDW interpolation method.

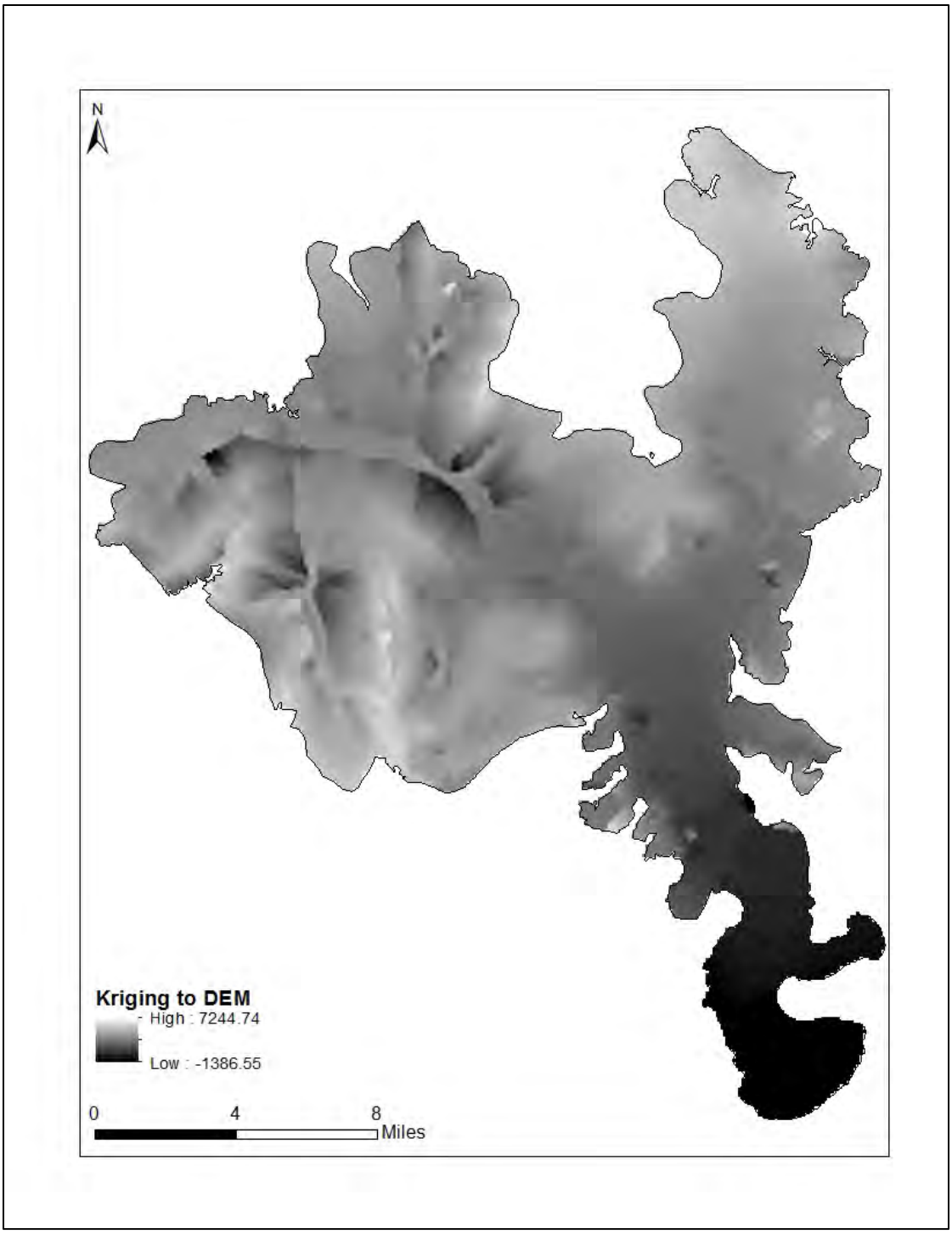

Figure 27 DEM (m) raster generated using universal kriging interpolation.

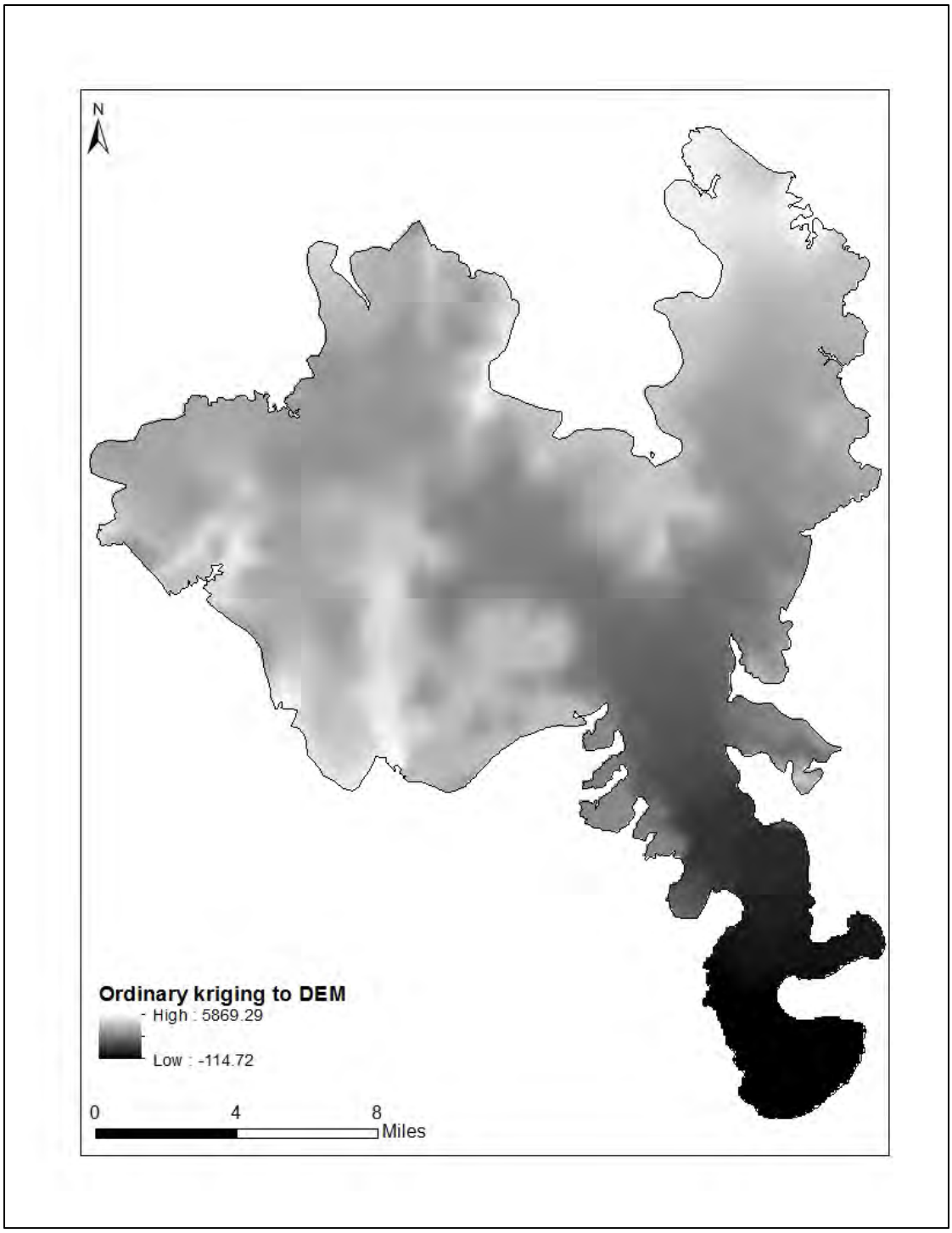

Figure 28 DEM (m) raster generated using ordinary kriging interpolation.

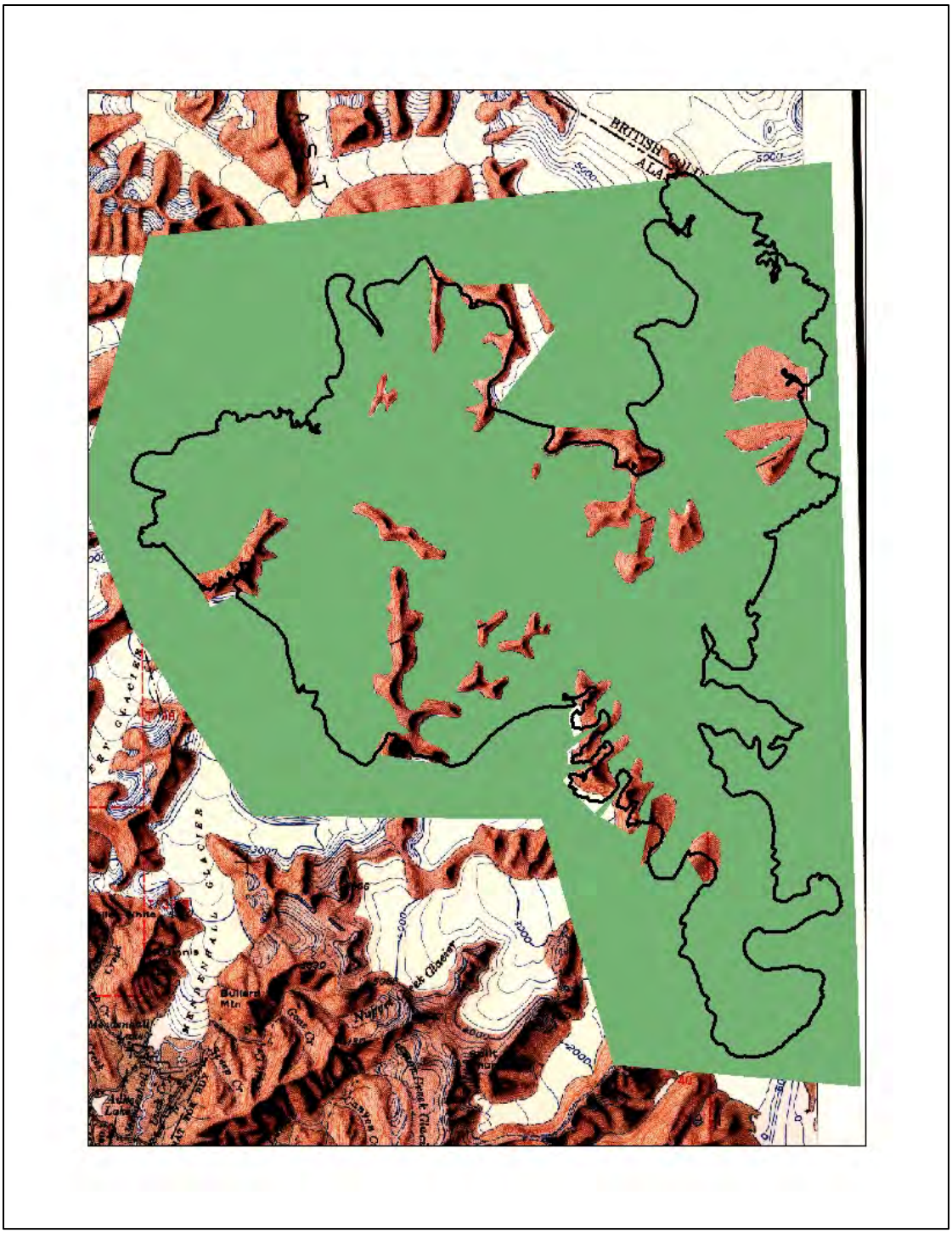

Figure 29 Map showing rough study area polygon excluding bedrock surfaces.

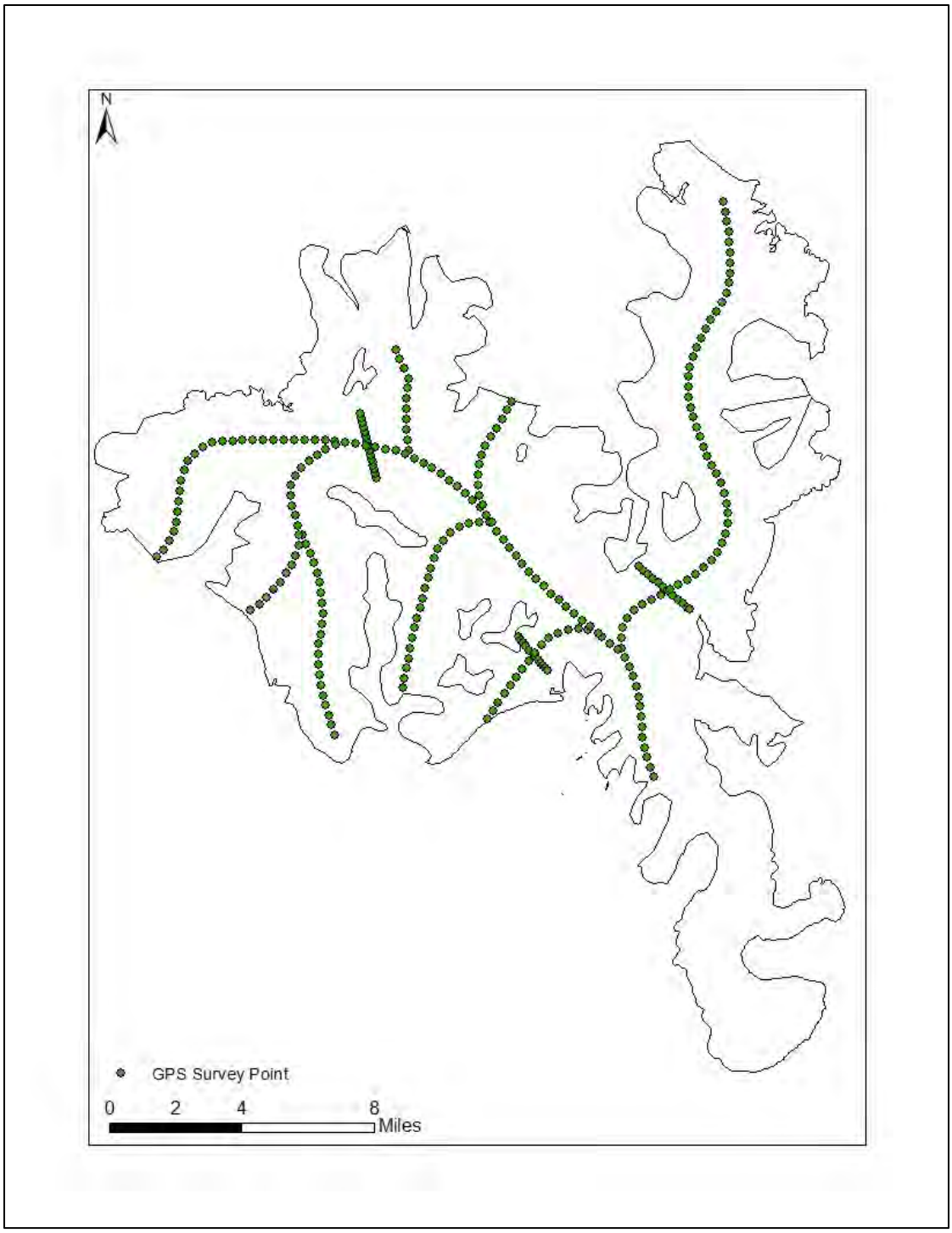

Figure 30 Eleven GPS survey profiles used to create DEM.

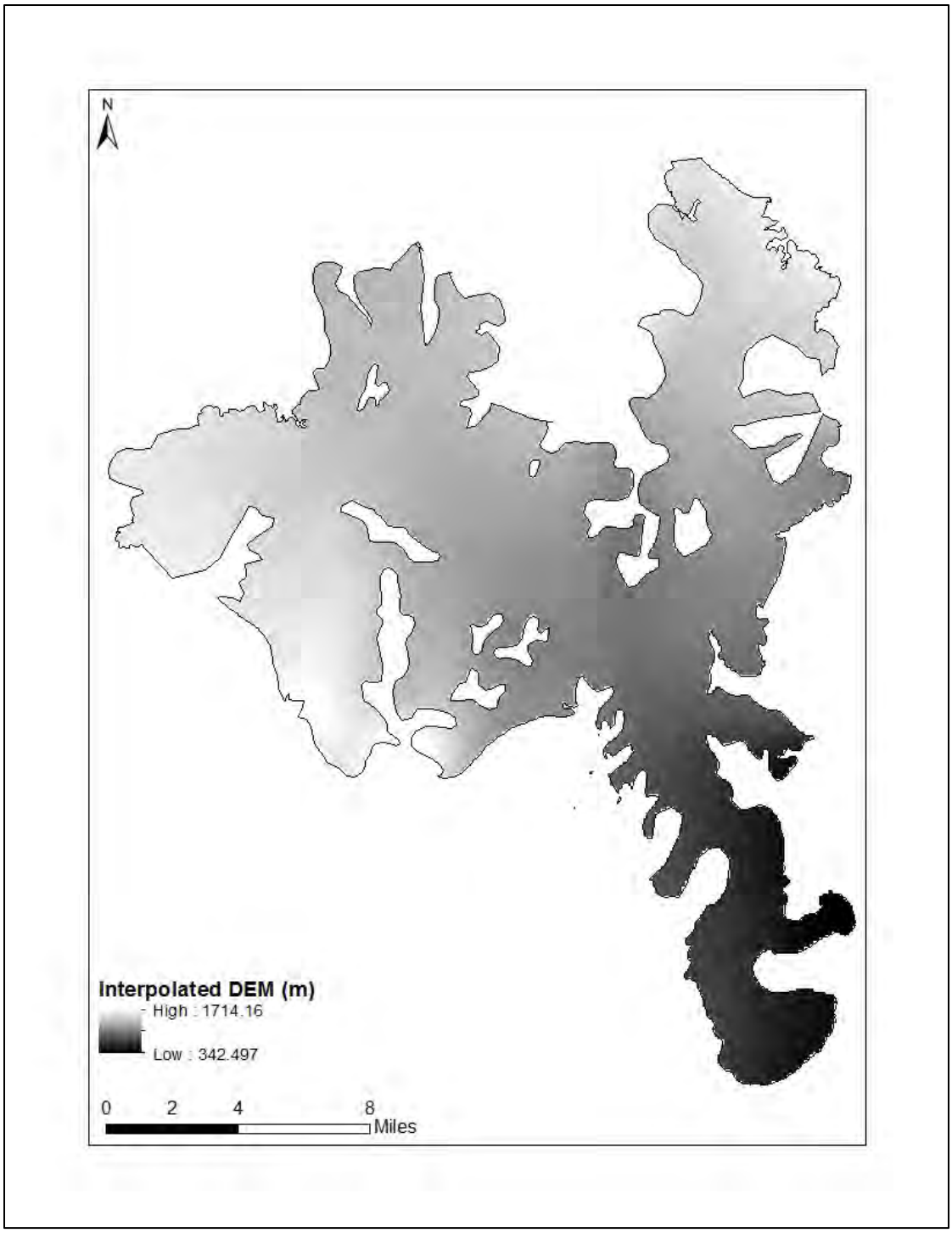

Figure 31 DEM created from GPS survey points.

Appendix D: Images associated with results of the elevation change analysis.

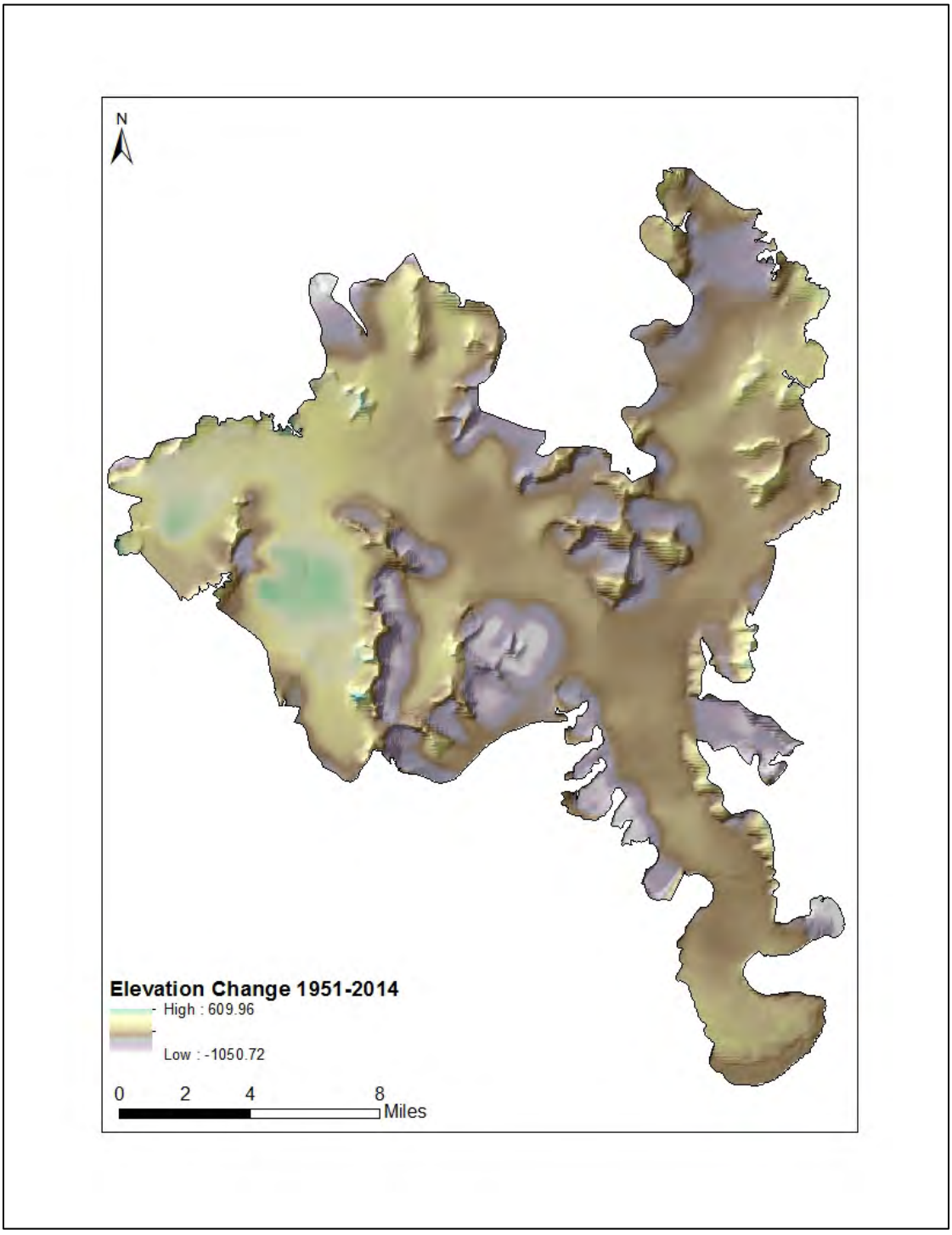

Figure 32 Map showing elevation change between 1951 and 2014 (m).

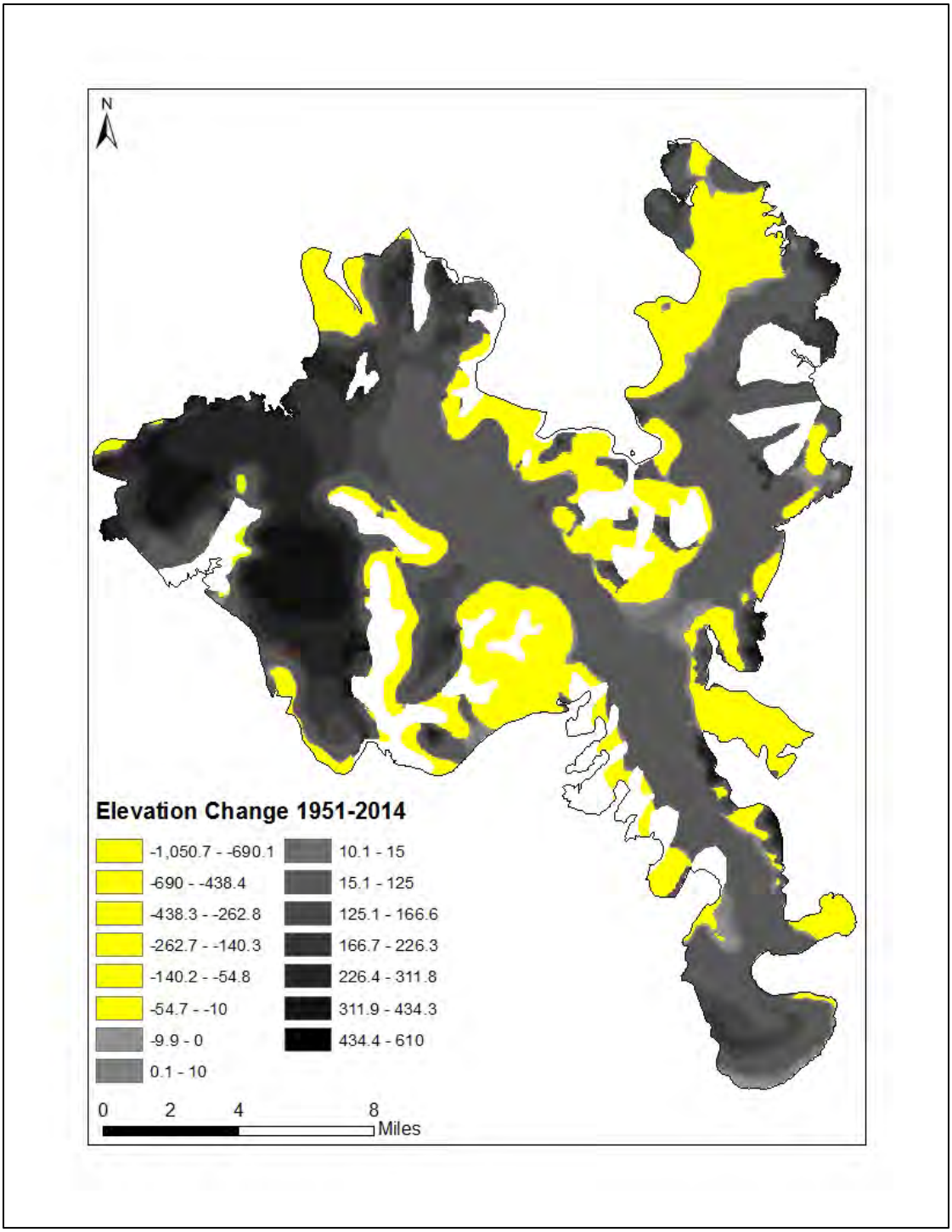

Figure 33 Map showing areas of highest elevation change (m) (yellow).

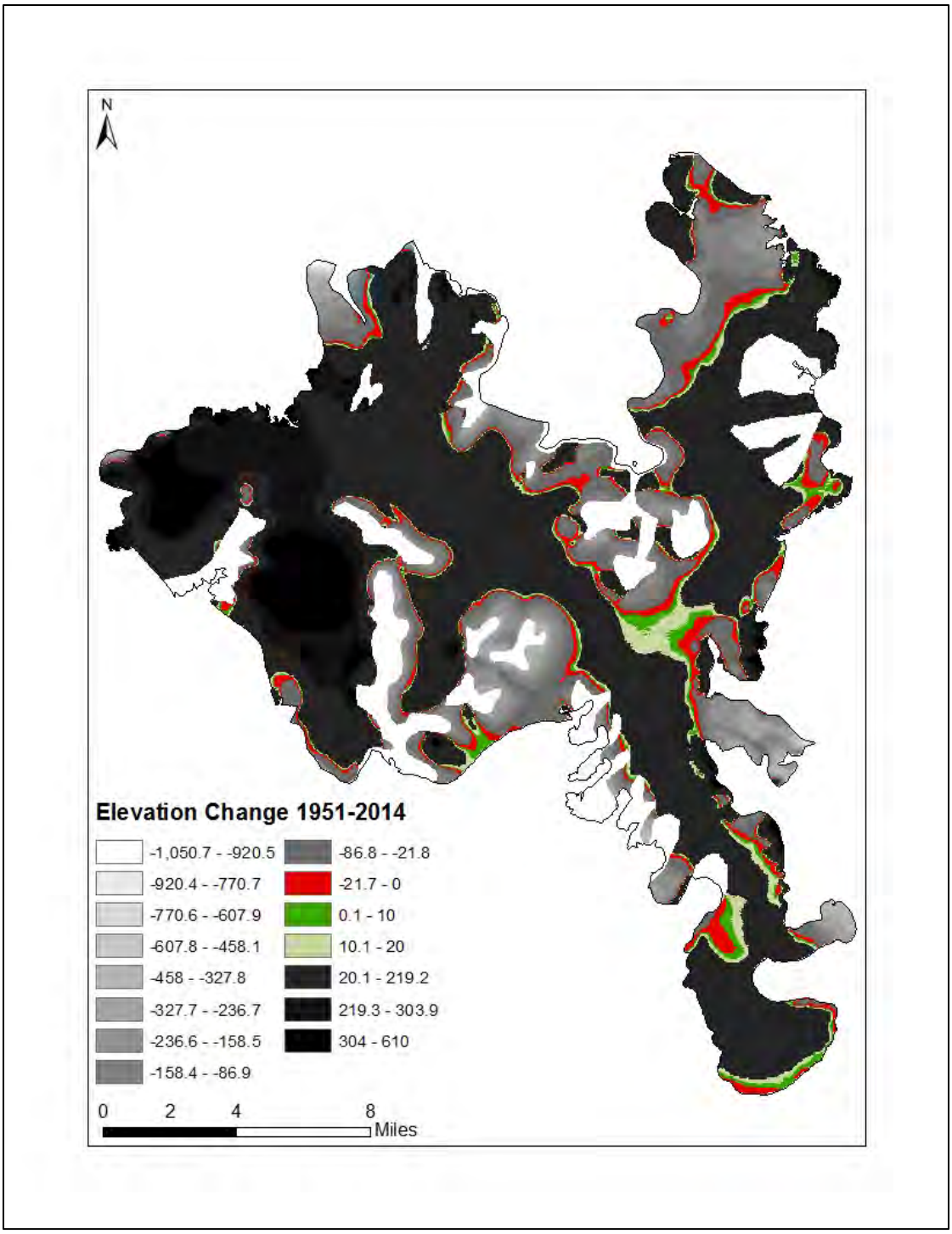

Figure 34 Map showing areas of elevation gain and loss (m) within a reasonable range of values observed from mass balance measurements.

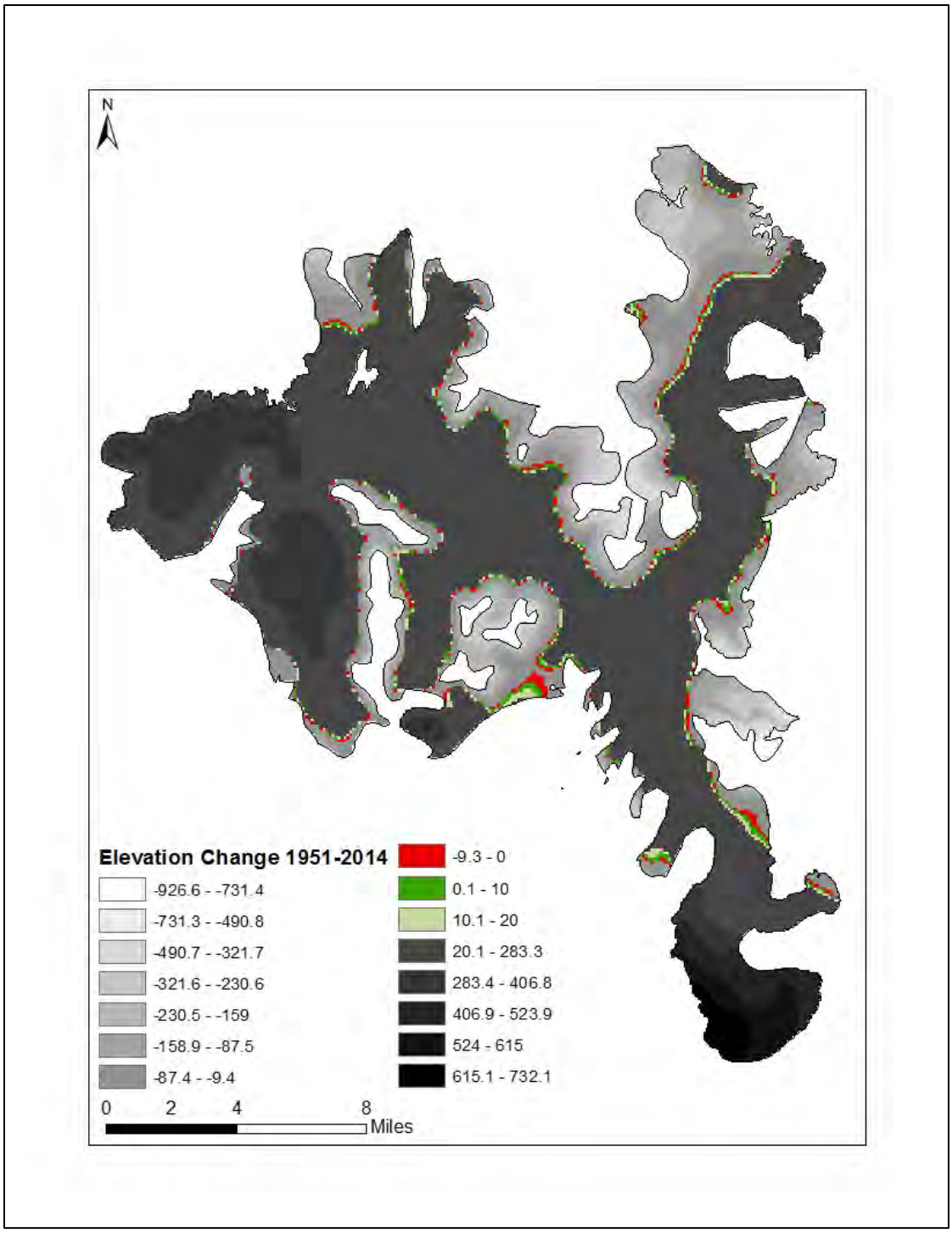

Figure 35 Map showing areas of elevation gain and loss (m) within the range of values observed from mass balance measurements.